The University Of Sheffield.

Department Of Mechanical Engineering.

Stall Control of a NACA0015 Aerofoil at Low Reynolds Numbers

Kanok Tongsawang

January 2015

A thesis submitted to the University of Sheffield in partial Fulfillment of the requirements for the degree of Master of Philosophy

Acknowledgements

Firstly, I would like to thank my supervisor, Dr. Robert J. Howell, for his invaluable guidance, time and continual support throughout my project.
Secondly, I would like to thank The Royal Thai Air Force for the financial support for my MPhil research.
Thanks are also due to the technicians from the Mechanical Engineering department for their valuable help and support.
Last but not least, I am very grateful to my parents and my wife for their encouragement throughout my study.

Abstract

This thesis focuses on experiments for stall control by using boundary layer trips on a NACA0015 aerofoil wing at low Reynolds numbers. Some simulation for a 2D aerofoil simulation was studied. The NACA0015 aerofoil simulation with different numbers of node and turbulence models at an angle of attack of 6 degrees was investigated for grid independence study. Then the mesh of 400 nodes around the aerofoil was chosen in simulation at various angles of attack. For the experiments, a NACA0015 wing with and without boundary layer trip at Reynolds number of 78,000 was conducted to determine the aerodynamic characteristics of the aerofoil in both cases and to determine the optimized values of the size and location of the boundary layer trips.

The results show that the wing with no trip stalled at the angle of attack of 14 degrees with C_{Lmax} of 0.78. As a result of the roughness of the wing, the interference drag between the wing and the struts and the induced drag from wing tip vortices, the total drag coefficient values are higher than that of the aerofoil. When the boundary layer trips were added to the wing, the results showed that lift coefficients of every BLT height located at 50%c from the leading edge are highest when compared to other positions. The results state that 6 mm height BLT located at 50%c produced lowest C_L while normal wing without BLT produced highest C_L for angles of attack between 0° and 14°. The BLT causes less severe stalling due to LSB reduction and reattachment resulting in more lift as the angle of attack increases to greater than 15°. Drag coefficients of BLT height of 6, 4, 3, and 1.5 mm located at 50%c from the leading edge were compared to the wing without BLT. The results indicate that 4 mm height BLT generated lowest C_D compared to all cases both the normal wing and the wing with BLT.

For CFD simulations at Reynolds number of 650,000, the 2D NACA0015 aerofoil simulations with different turbulence models shows that the Cl slope is in good agreement with the 2D experimental results(NACA report No.586) from 0° to 9° of angle of attack. The obvious difference can be seen after 12°. Stall angle of the turbulence models are higher than that of the experiment due to the mesh construction and the sharp trailing edge of the aerofoil in CFD simulation that is sharper than the aerofoil model tested experimentally.

Contents

List of figures

Nomenclature

a	Lift curve slope for a finite wing
a_0	Lift curve slope for an aerofoil
AR	Aspect ratio
BLT	Boundary layer trip
c	Aerofoil chord
C_f	Skin friction coefficient
C_l	Lift coefficient for an aerofoil
C_d	Drag coefficient for an aerofoil
C_L	Lift coefficient for a 3D flow
C_D	Drag coefficient for a 3D flow
C_{Lmax}	Maximum lift coefficient
C_p	Pressure coefficient
C_μ	Jet momentum coefficient
d	Diameter
e	Vortex generator length
f	Actuation frequency
F^+	Non-dimensional excitation frequency
h	Width of slot exit; Vortex generator height; BLT height
k	Roughness height
LSB	Laminar separation bubble
L_s	Length of separated region
M	Mach number
p	Pressure
q	Freestream dynamic pressure
Re	Reynolds number
U_*	Friction velocity
U_∞	Freestream velocity
V	Velocity
y	Wall distance
y^+	Non-dimensional wall distance
z	Distance between two pairs of vortex generators

Greek Symbols

α	Angle of attack of an aerofoil
β	Angle of incidence of a vortex generator
Γ^+	Positive vortex circulation
δ	Boundary layer thickness

δ_1	Boundary layer displacement thickness
Δ	Difference of
θ	Boundary layer momentum thickness
Λ_1	Pressure gradient parameter
μ	Dynamic viscosity
ν	Kinematic viscosity
ρ	Density
τ	Shear stress
τ_w	Wall shear stress
ω^+	Peak vorticity

Subscripts

e	External to the boundary layer at a particular location
p	Pressure
x	Downstream distance
w	Wall value

1. Introduction

1.1 Background

Flow separation on an aircraft or a wing can cause lift reduction and/or drag increment resulting in the performance of the aircraft as well as fuel consumption. Higher drag makes the fuel consumption greater and degrades the performance leading to loss of control in some circumstances.

Flow separation control provides many benefits such as lift/stall characteristics improvement, which lead to better performance due to a decrease in landing speed and increase in maneuverability. A number of active and passive flow control techniques in order to reduce or suppress the separation have been used for many years.

Passive flow control devices are the least expensive and the simplest solution to deal with the separation flow. They can be implemented in a range from subsonic to transonic flow. Vane-type vortex generators (VGs) are a method widely used because of their effectiveness and simplicity. These devices produce streamwise vortices downstream and induce momentum transfer between the freestream and the region close to the wall. Disadvantages of the vortex generators are parasite drag during the cruise and limited effectiveness in some operation range.

A blowing technique by injection of high momentum fluid into the low momentum boundary layer near the wall is used to prevent or delay the boundary layer separation in adverse pressure gradient zone. Nevertheless, this method needs a complex system for air compression process, which increases the gross weight of the aircraft affecting the aircraft performance and fuel consumption. The similar technique, the suction method, is a way to prevent or delay the separation effectively but it requires a complex internal vacuum system as well as the system is heavy so it is not practical to be implemented.

Synthetic jets (SJs) are a means of controlling the boundary layer separation. This method utilizes periodic excitation with zero net mass flux moving through an orifice, caused by a movement of a diaphragm in order to generate the periodic disturbance. The movement of the diaphragm causes suction and blowing strokes, which entrain the flow from outside the boundary layer into the near wall region, resulting in delaying or alleviating the separation flow. However, the optimization process is needs to maximize

their flow control effectiveness condition for the synthetic jet actuator operation.

There is a method to be implemented in order to reduce separation flow. That is boundary layer trips, which are a means of passive flow separation control. This method is not expensive and simple. To optimize the separation flow control by means of boundary layer trips, size and location of the devices are very important. At low Reynolds numbers, the laminar separation bubbles often cause an increase in drag on aerofoils. The use of boundary layer trips enhance the instability of the Tollmien-Schlichting waves leading to turbulent flow. The transition can cause reattachment of the separated laminar boundary layer due to its transition to turbulent flow. In addition, the laminar separation bubbles size is reduced, resulting in pressure drag reduction.

Many methods are useful to improve the flow to prevent, delay or suppress the boundary layer separation. This thesis was originally focused on synthetic jets and vortex generators as a means of control but for a variety of reasons, such as, time constraints, the objective changed to the study of the boundary layer trips. The literature review however still contains a significant amount of information about vortex and synthetic jet control. As mentioned before, boundary layer trips are not expensive and/or difficult to implement; therefore, the investigation of the effect of the boundary layer trips with different size of circular tubes and different locations on a NACA 0015 aerofoil wing was conducted at low Reynolds number of 78,000 in subsonic wind tunnel at the Mechanical Engineering Department, at the University of Sheffield.

1.2 Aims and objectives of the research

The aims of the current research are to achieve an improved aerofoil/wing performance at low Reynolds numbers by utilizing boundary layer trips to resist the laminar boundary layer separation and to determine the size and location of the devices which give the best performance with limited material and time. To achieve these aims, the objectives are as follows:

- To investigate the effectiveness of the boundary layer trip to flow separation control, especially in reducing laminar separation bubbles and in improving aerodynamic characteristics of the aerofoil/wing.
- To investigate the effect of size and location of the boundary layer trips on the NACA 0015 aerofoil wing at a low Reynolds number of 78,000 with various angles of attack.

2. Literature review

Various flow control techniques are used to manage flow around aerodynamic bodies to increase the performance of the objects. These can delay separated flow in order to reduce drag, enhance lift and stall the angle of attack in cases of aircraft wings; in addition, they provide mixing augmentation and flow induced noise suppression [6]. Boundary layer concept was presented by Prandtl in 1904 [100]. He explained the physics behind the flow separation and demonstrated some experimental results where the boundary layer was controlled by applying a blowing jet around a circular cylinder to delay flow separation [8, 9, 6]. The boundary layer separation indicates losses of great energy and limitations of the aerodynamic performance of an aircraft. Hence, the control of the boundary layer is still a major task for the aerodynamicists. In the military, active flow control is used by using complex steady jets and this requires large power [10, 11, 12].

Control surfaces of a transport aircraft such as flaps, ailerons generate not only give extra lift they also generate extra drag. Most of these control surfaces use passive flow control to control the flow over wings. The passive flow control means that the flow control is applied only by deflecting the control surfaces and no energy is added to the flow [8]. The effectiveness of the control surfaces at a high angle of attack decreases due to flow separation and this problem can be fixed by applying flow control method. This approach can control the flow; besides, this can retain the aerodynamic efficiency.

The flow control could be implemented on an aircraft wing at various positions shown in Figure 2.1. While taking-off and landing leading and trailing edges separation control could be used to reduce the pressure drag and as cruising laminar, transition and turbulence flow control could be utilized.

Flow separation can be induced by strong adverse pressure gradient which affects boundary layer to separate from wing surface. Leading edge devices (slat) and trailing edge devices (flap) are used to delay the separation flow and to enhance the performance of an aircraft by increasing lift coefficient during the take-off and landing.

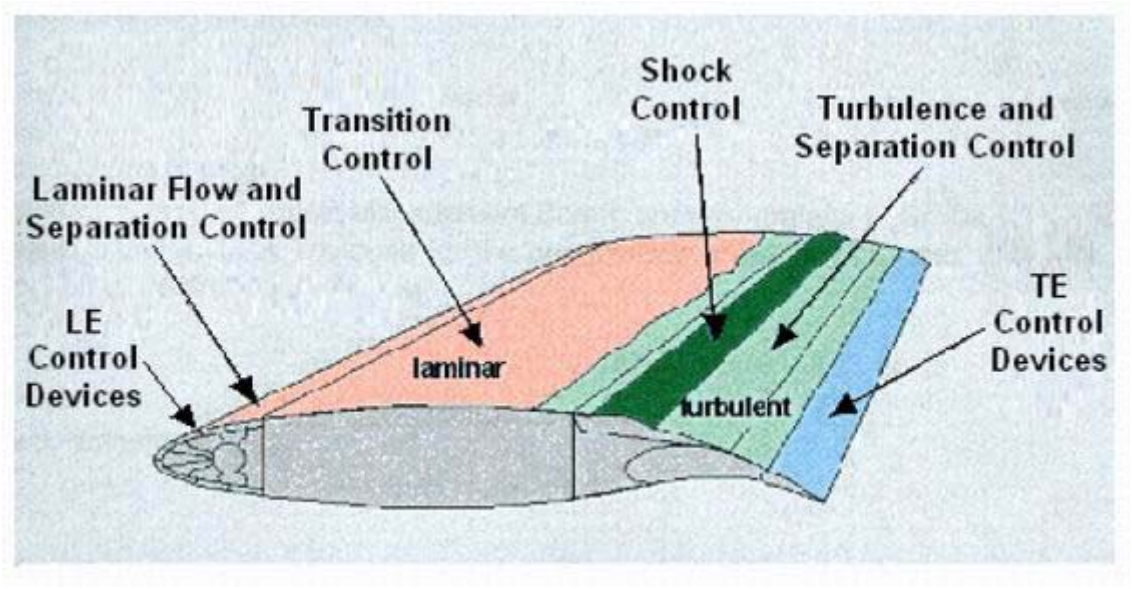

Figure 2.1 Schematic for flow control regimes for an aircraft wing [87]

Flow control techniques can be divided into two main groups using different schemes which are passive and active flow control.

Passive flow control techniques, either macro overturn the mean flow using embedded streamwise vortices produced by fixed lifting surface or amplify Reynolds stress which increases the cross-stream momentum transfer, and these received great attention during the 1970s and 1980s.

Passive control by blowing through leading-edge slats and trailing-edge flaps is a feature of some high-lift systems. When the high-lift systems are deployed, the air from the lower surface of the wing element passes over the upper surface which injects the high momentum fluid so energize the boundary layer. Although the pressure difference between the upper and lower surface can limit the efficiency of the devices, this method can significantly affect the lift and drag on the body [94].

The best known vortex generators (VGs) are a conventional passive control technique dating from the 1940s [30]. The VGs generally consist of, for instance, small rectangular, triangular or trapezoidal vanes of approximately boundary layer height in arrays and are set at incidence to the local velocity vector. The VGs may generate an array of co-rotating vortices, or pairs of counter-rotating vortices depending on their configuration. The generated vortices entrain higher momentum fluid from the outer region of the boundary layer to the near-wall region and enhance the resistance of the boundary layer to separation. The advantages of the VGs are their low weight, robustness and simplicity making them widely used. They control flow separation effectively; however, the conventional VGs of the height of the

order of the boundary layer thickness δ, produce important parasitic drag. A means to improve the performance of VGs is to reduce the height of the VGs from the order of δ to 0.2δ or less [38, 53, 54]. The devices named submerged VGs [55], sub boundary layer VGs [59], low-profile VGs [36], and micro VGs all have smaller order of the height than the conventional one.

The micro VGs still produce an array of small streamwise vortices to overcome the flow separation, but with reduced parasitic drag. However, VGs have some shortcomings. They do not have the ability to provide a time-varying control action and therefore they are only effective over a small operational range. Furthermore, the parasitic drag produced by VGs is inevitable [56].

Since the 1990s, active flow control has been widely researched instead of passive flow control. Active flow control with a control loop is divided into predetermined and reactive categories. Predetermined control is an open control loop because it inputs steady or unsteady energy without regarding the particular state of the flow. On the other hand, the control input of reactive control is adjustable based on the measurements of sensor, and the control loop can either be open feedforward or closed feedback. The distinction between feedforward and feedback is that the controlled variable differs from the measured variable for feedforward control, but it must be measured, fed back and compared with a reference input for feedback control [99].

The primary advantages of active flow control over passive flow control were summarized by Kral [96]. Firstly, active flow control can control a natural stability of the flow effectively by the expense of small, localized energy input. Secondly, active control can be operated on demand when needed, and its input power level can be varied according to the local flow condition. Active flow control techniques include wall jets, wall transpiration (suction), and vortex generating jets. Wall jets, similar to passive blowing, inject fluid tangentially to the boundary layer to enhance the shear layer momentum.

Separation control by blowing at high speed is covered in the reviews by Delery [95] and Viswanath [101]. Wall transpiration or steady suction can be applied through porous surfaces, perforated plates, or carefully machined slots. The effect of suction in preventing flow separation from the surface of a cylinder was first tested by Prandtl [100]. Its remarkable effect was demonstrated on a variety of wind tunnel models and in flight tests [97]. Nevertheless, the disadvantages of both techniques are the complexity of the internal piping to generate the high pressure as well as the large weight. In addition, the aerodynamic benefits obtained by both methods are probably

offset by the power required to operate these devices. These are the reasons that they are impractical for many applications.

Vortex generator jets (VGJs) are believed to produce an effect similar to VGs because they generate longitudinal vortices from discrete orifices to enhance fluid mixing in the near-wall region. They were first proposed and studied by Wallis [102]. According to the different jet orifice orientation to the main flow, VGJs can generate arrays of counter-rotating longitudinal vortices (normal jets) or co-rotating longitudinal vortices (pitched and skewed jets), which are similar to that produced by VGs.

Steady jets and pulsed jets are two typical types of VGJs which have been studied extensively [53, 54]. The pulsed jets, using oscillatory or intermittent momentum addition, especially, have obtained more attention recently, because they have a similarly capability to steady jets but with reduced net mass flux. The effectiveness of steady jets versus pulsed jets for the delay of stall on a thin aerofoil was compared by Seifert et al. [10]. For the same improvements in lift, the pulsed jets were found to require less momentum C_μ = 0.3%, in comparison to the steady jets, C_μ = 3% (where C_μ is the momentum coefficient, defined as the ratio of jet momentum to the local freestream momentum). Johari and McManus [98] showed that the pulsed jets reduce the mass flow rate and enhance the vorticity and the boundary layer penetration at the same velocity ratio as compared to the steady jets. However, both steady jets and pulsed jets require the complex internal piping system.

To avoid the complex piping system while maintaining all the other advantages of pulsed jets, Synthetic jets (SJAs), a means of periodic excitation with zero-net-mass-flux, have been proposed and attracted attention in recent years. The primary advantage of SJAs is that they do not require air supply and the weight penalty is smaller compared to the steady and pulsed jets. In addition, they can transfer non-zero momentum to the external fluid, and generate coherent vortices which can provide a favourable control effect. Furthermore, SJAs use external fluid for jet production, spending smaller amount of the energy, and can be made compact. Thus, SJAs have been applied to high-lift systems for flow separation control [76]. SJAs have the potential for Micro-Elector-Mechanical Systems (MEMS) which open up a new territory for flow control research. Such systems having micron-sized sensors and actuators, and integrated IC with micro transducers, can execute sense-decision actuation on a monolithic level, therefore they could reduce the potential density of the actuator systems in the wing, and more importantly, meet a prerequisite for aircraft implementation [103]. It is because the local boundary layer thickness is of the

order of 1 to 3 mm on the leading edge devices, and 1 to 10 mm on the trailing edge at the take-off condition, depending on the size of the aircraft. Therefore, considering the boundary layer thickness in practice, it is required to apply MEMS based micro-scale SJAs. However, there are some practical problems with using synthetic jets at flight scale. First, a very high driving frequency is required to establish a synthetic jet in time to control the near-wall streak structures individually, which is at least an order of magnitude greater than the turbulent bursting frequency. Second, synthetic jets must have several diaphragm cycles to establish itself that places a limit on their speed of response for controlling the streaks in a turbulent boundary layer. Last, the small size of orifice makes dirt or debris block it easily, especially during the suction stroke. It is a serious issue for aircraft manufacturers since cleaning MEMS would be a demanding operation. The effectiveness of SJAs in delaying flow separation has been proved by a number of investigations in the laboratory [20, 24, 76, 77, 104].

Wood et al. [104] investigated the flow control effectiveness of an array of circular synthetic jets normal to the surface of a circular cylinder model upstream of its separation line in a turbulent boundary layer ($Re = 5.5\times10^5$ based on the cylinder diameter). Oil flow visualization indicated that longitudinal vortices were developed and persisted for a long distance downstream as a result of the interaction between the synthetic jets array and the turbulent boundary layer, and therefore the separation line was pushed downstream where the synthetic jets were actuated upstream. Although the capability of SJAs in delaying flow separation has been demonstrated in various manners, the understanding of the physical process, especially the formation of vortex ring, its interaction with the boundary layer and its impact on the near-wall region is still important, which will be helpful to design and select suitable SJAs in practical application. For SJAs, a number of issues need to be addressed in terms of compactness, weight, efficiency, control authority, and power density. Hence, it is not easy to design and get the effective SJAs for many applications.

At the beginning, the flow control techniques in this project focused on synthetic jets (SJAs), passive vortex generators (VGs), and boundary layer trip (BLT). For time constraint reason, the project currently focuses on only the boundary layer trip. However, the literature review has still included the synthetic jets and vortex generators. These three flow control techniques are as follows:

2.1 Synthetic jets

Flow control aims to modify the flow to enhance the ability of the wings to function at extreme attitudes [2]. Active flow control has the ability to change the lift coefficient without changing the angle of attack or deflecting the control surfaces. The word active implies the addition of energy to the flow [13]. Both suction and blowing are some of the active flow control techniques that have been used to improve flow quality. These methods change the shape of the aerofoil virtually and have the potential to avoid the flow separation. However, suction or blowing type actuators require large amount of power and space. They are also mechanically complex, making them practically difficult to implement [14, 15].

Recently, the synthetic jet or Zero Net Mass Flux (ZNMF) method has been introduced. The Zero Net Mass Flux (ZNMF) jet is created by oscillating the fluid around the aerofoil periodically. The net mass flux is zero because of periodic sucking and blowing of the air surrounding the jet orifice. The synthetic jet induces zero net mass flux; however, it generates momentum that changes the behaviour of the flow. The synthetic jet is created by driving one side of the cavity in a periodic manner. There are many methods to generate the synthetic jet such as use of driven pistons, speakers, driven diaphragms [16]. These do not require extra fluid because the fluid around the aerofoil is driven mechanically or using electric power. The synthetic jet creates an oscillatory periodic flow sucked or blown through an orifice. Figure 2.2 is the sketch of a synthetic jet actuator. In the suction phase, the fluid is moved into the cavity and in the blowing phase the fluid is driven out of the cavity and forms a vortex pair. As the vortex pair moves away from the orifice, the diaphragm sucks the fluid into the cavity and in the blowing phase, a new vortex pair is created. The generated vortex pairs interact with the separated flow region and cause low pressure region in the interaction zone. The low pressure region around the synthetic jet causes partial or complete reattachment of the flow. Reattachment of the separated flow results in the reduction in pressure drag [17].

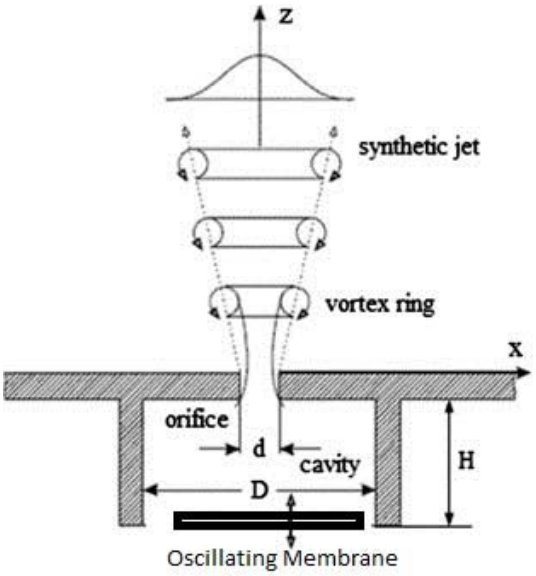

Figure 2.2 Schematic representation of the synthetic jet actuator

The active flow control using synthetic jet is becoming an active research field because of its advantages compared with the conventional flow control using lifting surfaces such as flaps, slats etc. [5]. Effectiveness of the conventional control decreases as the angle of attack increases; on the other hand, the synthetic jet changes the shape of the aerofoil virtually and it can be used at high angles of attack due to the reattachment of the separated flow. The size of active flow control devices is small and their weight is light compared to conventional control devices [14]. In addition to preventing the flow separation, the active flow control delays the transition of a laminar boundary layer to a turbulent boundary layer [18]. If the active flow control technique could be used effectively, there would be no need to use the conventional control surfaces which cause significant weight penalty [5].

Experimental and computational studies show that if the synthetic jet is applied properly, the aerodynamic performance of aerofoils can be increased in terms of lift enhancement and drag reduction [20, 11, 12, 13].The active flow control methods can also be used in transition delay, separation postponement, turbulence augmentation and noise suppression [20, 21, 15]. As the laminar boundary layer separates in the flow, a free-shear layer forms and transition to turbulence takes place at high Reynolds numbers. Increased entrainment of high-speed flow due to the turbulent mixing may cause reattachment of the separated region and formation of a laminar separation bubble. At high incidence, the bubble breaks down either by a complete separation or a longer bubble. In both cases, form drag increases and causes a reduction in the lift-curve's slope [7]. All these physical phenomena should

be considered together in use of active flow control and these make active flow control as the art of flow control [19].

Understanding the physics behind the synthetic jet interaction with the flow over an aerofoil requires a lot of experiments. Using a numerical simulation is a way to reduce cost. Numerical simulation can provide a wider understanding inside the control mechanisms [22]. There are numerous studies in active flow control field especially in the last decade. Recent experimental and computational studies carried out for flow control investigated the effect of synthetic jet on the flow over aerofoils. There are many studies that only concern the behaviour of synthetic jets. In the study of Utturkar et al. [23], numerical simulations are performed to define the velocity profiles of two-dimensional axisymmetric synthetic jets. Lee and Goldstein [1] have performed Direct Numerical Simulation (DNS) solutions to model synthetic jets. The results of the numerical study are compared with the experimental data of Smith [24].

In the study of Mallinson et al. [15], the flow over an aerofoil produced using a synthetic jet becomes periodic more rapidly than the flow over an aerofoil with a steady jet. It is reported that the rapid establishment of the synthetic jet is caused by turbulent dissipation, which keeps a vortex near the orifice, thus limiting the size of the turbulent core.

In the study of Lance et al. [2], an experimental study was performed to evaluate the effectiveness of a synthetic jet actuator for the flow control on a pitching aerofoil. The exit slot area is dynamically adjustable and the exit is curved such that the jet is tangential to the surface, taking the advantage of Coanda effect. The synthetic jet actuation parameters included the jet momentum coefficient and the slot exit width. In all experiments, the aerofoil was pitched from 0°to 27°at a constant angular velocity in 1 second. The results of the experiment have shown that synthetic jet actuation delays the formation of the dynamic-stall-vortex to higher incidence angles.

Hamdani et al. [25] have studied the flow over NACA 0018 applying alternating tangential blowing/suction. The active flow control is found to be ineffective for attached flows. Nevertheless, suction is found to be more effective than blowing. The boundary layer profile of suction is fuller both at the upstream and downstream of the slot. This is the reason why the suction is more effective than the blowing. In that study, the jet location is varied and the effectiveness of the jet at these locations is investigated. The results show that the slot location is a very important parameter for separation control. It is observed that when the jet slot is located before 75% of the chord, the

control is effective but it becomes ineffective when the slot is located at 0.75c which is at the downstream of the separation point. Seifert et al. [10] have tested different multi-element aerofoils using an oscillatory blowing jet in order to prevent separation that occurs at increasing incidence. They have shown that when the flow separates from the flap, not from the main body, the blowing from the shoulder of a deflected flap is much more effective than blowing from the leading edge. According to that study, application of an oscillatory blowing jet can be used instead of a conventional control because it requires low power and it is simpler to install compared to steady suction jets.

Martin et al. [3] have researched helicopter pylon/fuselage drag reduction by active flow control. A thick aerofoil, NACA 0036 is chosen as baseline 2D test geometry. The results show that the flow separates even at 0^{o}angle of attack. Separation is much more severe at 10^{o}angle of attack. When the flow control is applied, the displacement thickness of the separated shear layer was reduced and separated bubble was close to the trailing edge.

One application of the synthetic jet is to use it in Unmanned Air Vehicles, UAV. Parekh et al. [26] have applied the synthetic jet concept over the wings of a UAV. The research has shown that the turn rate was increased by controlling the leading edge separation. Patel et al. [14] indicate that as the synthetic jet technology improves, active flow control can be used in the development of UAVs without conventional control surfaces.

The synthetic jet is implemented in a concept car named as the Renault-Altica. The synthetic jet is located at the edge of the rear roof at which the flow separates from the vehicle. Jets of air are alternately blown and sucked through a 2mm wide slot. The drag is reduced by 15% at 130 kph with an energy consumption of just 10 Watts. The thickness of the separated flow region at the base of the car also decreases when the synthetic jet is applied [4].

The Aircraft Morphing program at NASA Langley aims to design an aircraft using synthetic jets. As a part of this program, a NACA0015 profile was tested in a wind tunnel experiment. The two-dimensional NACA0015 model has the dimensions of a 91.4 cm span and 91.4 cm chord. There are six locations over the model for the installation of the synthetic jet. Experimental results have shown that the effect of the synthetic jet decreases when the actuation is applied under the separated flow region [5].

Vadillo [17] has studied numerically on a 24% thick Clark-Y aerofoil by employing a synthetic jet. It was found that the maximum drag reduction with the minimum lift change occurs at higher frequencies of the synthetic jet. In the case of Wang et al. [27], the active flow control is applied to a NACA 633-018 aerofoil at a stall angle of attack. It is found that the most effective excitation frequency is about 1.5 to 2 times of the natural frequency ($U\infty/c$). At downstream after the separation point the synthetic jet is less effective. In addition, the effect of excitation on lift and drag reduces when the jet is excited at a lower intensity.

Numerical investigation of the active flow control using steady and synthetic jets over NACA0012 and NACA0015 aerofoils was undertaken by Donovan et al. [13]. Navier-Stokes computations with Spalart-Allmaras and SST turbulence models were used and compared with the experimental data. Both models show very good agreement before the stall. For the controlled case, the computational results do not agree with the experiment. It is observed that for attached flow, actuators change the aerodynamic shape by virtually changing the camber. For separated flow, the primary benefit of the actuator is reported to be reattachment of the separated flow partially. The studies over NACA 0012 aerofoil showed that the actuators placed near the leading edge had a stronger effect than the actuators placed farther aft.

Huang et al. [22] performed a numerical simulation using suction and blowing control over a NACA 0012 aerofoil at a Reynolds number of 500,000 and at an angle of attack of 18°. They changed three jet parameters; jet location, amplitude and angle. The results showed that suction has the advantage of creating a lower pressure on larger area over the upper surface of the aerofoil. Thus, the flow is more attached, lift is enhanced and the profile drag is reduced. Leading edge blowing increases the lift by generating greater circulation, but it significantly increases leading edge pressure; therefore, the flow is more detached resulting in profile drag increase. Downstream blowing can improve the lift and drag characteristics, but smaller amplitudes are better than larger ones. Moreover, larger amplitude blowing results in larger impact on the flow field around the aerofoil. For perpendicular suction, the optimum control amplitude range is between 0.01 and 0.2. The values exceeding 0.2 no longer manipulate the separation bubble for perpendicular suction. For downstream tangential blowing, smaller blowing amplitudes appear to be more effective.

Amitay [76] demonstrated the ability of SJAs for suppressing flow separation on symmetric aerofoil which has Reynolds numbers from $3.1\text{x}10^5$ to $7.25\text{x}10^5$ based on the chord. Two rectangular SJAs operate to produce synthetic jets.

The aerofoil stalls at angle of attack greater than 5 degree with no use of SJAs but when using the SJAs the stall angle can extend up to 17.5 degree. It has been proved that the location and the strength of the synthetic jet affect the extent of the reattached flow. To optimise the performance of the aerofoil, the location of the synthetic jet and momentum coefficient, C_μ, has to be investigated for wide range of angles of attack.

A factor that is important for controlling the efficiency of the SJA is the actuator operating frequency, which is always in the form of non-dimensional frequency, F^+, which is defined as $F^+ = fL_s/U_\infty$(f is the actuation frequency, L_s is the length of the separated region and U_∞ is the freestream velocity). Another parameter that is always used for SJA is jet momentum coefficient, which is defined as $C_\mu = \frac{h(\rho U_{max}^2)}{c(\rho U_\infty^2)}$ (h is the width of slot exit, c is the chord length, U_{max} is the maximum exit velocity).

Donovan et al [13] studied the sensitivity of the attached flow to the excitation frequency numerically. The simulation of NACA 0012 aerofoil using time-harmonic zero mass flux blowing at St =1 shows 20% increase in lift at α =22 º.

McCormick [77] conducted the leading edge separation control effectiveness of synthetic jet on a two-dimensional aerofoil section. The SJAs were located at 4% chordwise position of the leading edge separation, approximately 8%c. The slots inclined 20º from the surface. The Reynolds number of 2.5×10^5 and the actuation frequency of 50 Hz were set for the test. Three momentum coefficients, C_μ, the ratio of the orifice momentum to freestream momentum, were set to visualize the flow as illustrated in Figure 2.3. At C_μ= 0 or no actuation, the flow separated from the leading edge, shedding vertical structures in the shear layer as the picture sketched. At C_μ= 0.005, the flow much more turned and there were three vertical structures over the aerofoil which were locked to the forcing effect. At C_μ= 0.01-0.015, the flow was attached with no coherent structures. At higher C_μ (0.04-0.068), vortical structures again occurred, but of the opposite sense. This flow behaviour is more analogous to the synthetic jet in quiescent air and is clearly above the optimal forcing level.

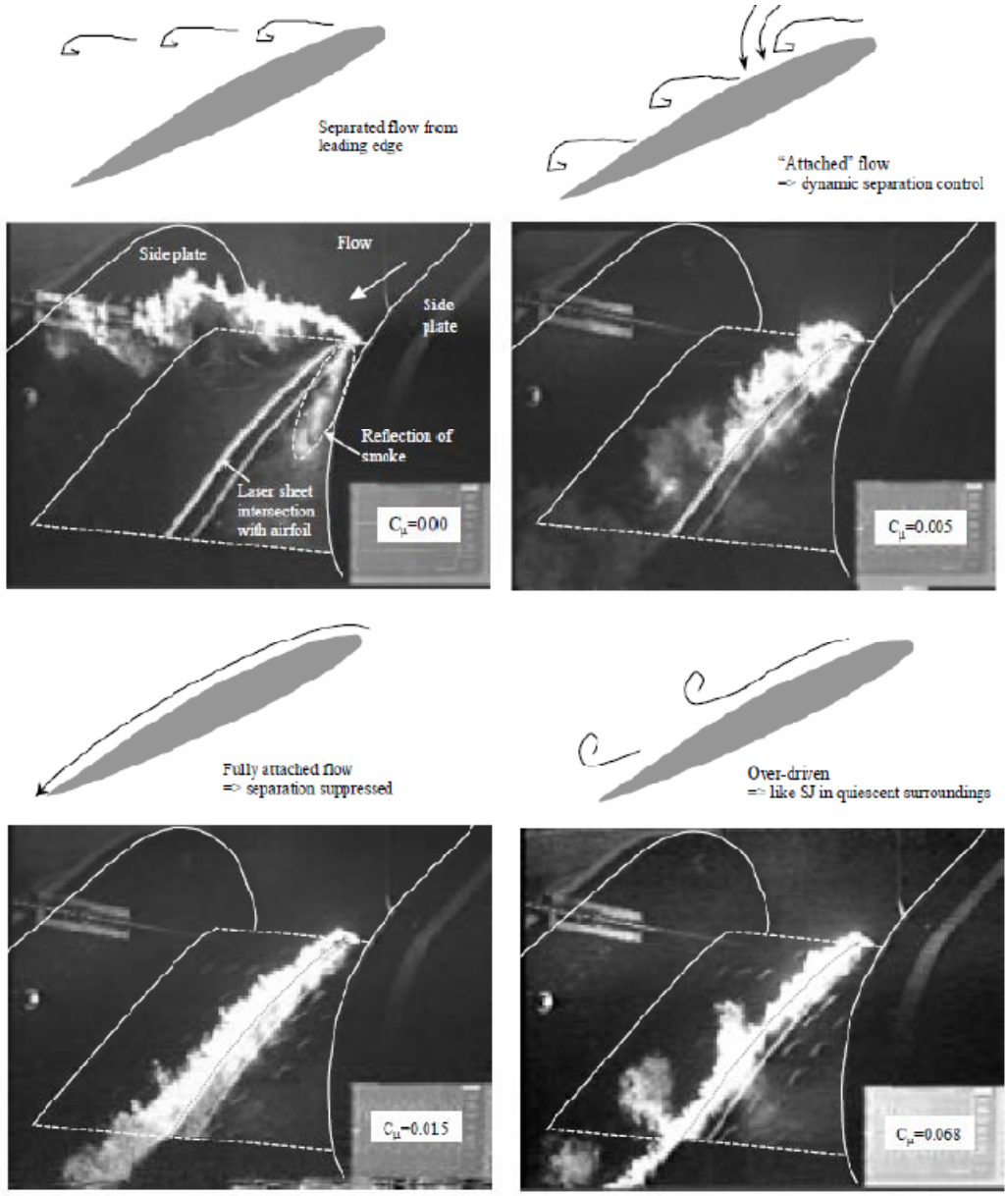

Figure 2.3 Flow visualization of flow separation control at different conditions [77]

Gilarranz et al [78] investigated application of SJAs to flow separation control over a NACA 0015 wing. The exit slot of the actuator was placed at 12%c from the leading edge. All of the reported tests were performed at a freestream velocity of 35 m/s or Re = 8.96×10^5. The angle of attack was varied from -2 deg to 29 deg. It is found that the actuator has minimal effect when operated at α lower than 10°. At higher degree, the actuator could delay the onset of stall. The frequencies of the actuation tested were between 60 Hz and 130 Hz according to F^+ between 0.57 and 1.23. The momentum coefficients tested were between 0.0051 and 0.0254 depending on the maximum jet exit velocity.

The use of the actuator results in an 80% increase in maximum lift coefficient and an extension of stall angle from 12º to 18º.

Tuck [75] investigated the effect of 2D micro zero-net-mass-flux (ZNMF) jet located at the leading edge of a NACA0015 aerofoil to enhance lift and control separation flow actively. Experiments were conducted in a water tunnel at a Reynolds number of 3.08×10^4 for a 2D aerofoil and a Reynolds number of 1.54×10^4 for flow visualization by MCCDPIV. The optimum forcing frequencies for active flow control using a wall-normal ZNMF jet located at the leading edge of the aerofoil were F^+ =0.7 or 1. When a forcing frequency of F^+=1.3 is used the most effective momentum was found to be C_μ= 0.14 per cent, which gives the highest lift coefficient. Using these forcing parameters the stall angle is extended from 10º to 18º and maximum lift coefficient is increased by 46% above the uncontrolled case.

2.2 Vortex generators

Early use of vortex generators is conventional passive vortex generators (VGs), especially vane-type with device height, h, on the size close to the local boundary-layer thickness, δ. A concept is to control separated flow by increasing the near-wall momentum by transferring higher-momentum flow from outside the boundary layer to the wall region. Taylor [30] introduced the conventional vortex generators in the late 1940s. The devices composed of a row of small plates or aerofoils normal to the surface with angle of incidence, β, to the local flow, resulting in streamwise trailing vortices. The purpose of these devices was to delay boundary-layer separation [31], to increase aircraft wing lift [32, 33], to reduce drag of aircraft fuselages [34], and to avoid or delay separation in subsonic diffusers [35]. Although the conventional VGs are widely used and work well for separation control, they may give more drag due to momentum conversion of aircraft into unrecoverable turbulence in the aircraft wake [36]. An appropriate VG is needed for certain application and need not produce too strong vortices downstream the flow causing more device drag. For this reason, low-profile vortex generators (micro-vortex generators) are widely used to reduce device drag.

Kuethe [37] improved and inspected non-conventional wave-type VGs with h/δ of 0.27 and 0.42 which use the Taylor–Goertler instability to produce streamwise vortices over a concave-surface flow. These VGs suppress the Kármán vortex street formation, alleviating acoustic disturbances and reducing the area of velocity deficit in the wake. Rao and Kariya [38] suggest that submerged VGs with $h/\delta \leq 0.625$ have a performance better than that

of conventional VGs with $h/\delta \sim 1$ because of the much lower device (or parasitic) drag. These result in the development of smaller VGs compared to the conventional vane-type VGs height. The VGs with $0.1 \leq h/\delta \leq 0.5$ have been approved to provide adequate momentum transfer over a region for effective flow separation control and they are called "low-profile VGs" [36]. As well as the low-profile VGs having less device drag, they can be stowed within the wing when not needed in some case and have lower radar cross section. The VGs provide many benefits, for instance, improvement in aerodynamic characteristics of a low-Reynolds number aerofoil [39], high-lift aerofoils [40,41], highly swept wings [42-46], a transonic aerofoil [47], aircraft interior noise reduction at transonic cruise [48], reduction of inlet flow distortion within compact ducts [49-51], and a more efficient overwing fairing [52].

The NASA Langley Research Center conducted flow-control experiments in the late 1980s. The experiments were based on the flow over a two-dimensional 25°sloped, backward-facing curved ramp at a wind speed of 132 ft/s [53–56]. The most effective results of various types of passive flow-control devices are summarized in Figure 2.4(a) in the percent reduction of the separated-flow region. The figure shows that the devices which generate streamwise vortices are the most effective devices for flow-separation control, such as those produced by the low-profile VGs, conventional VGs, and large longitudinal surface grooves. Lin et al. [53-56] examined counter-rotating and co-rotating vane-type VGs as well as Wheeler's doublet and wishbone VGs (Figure 2.4(b)). The VGs with $h/\delta \sim 0.2$(sub-δ-scale) are found to be as effective as the conventional VGs with $h/\delta \sim 0.8$h (δ-scale) in delaying flow separation. The devices generating transverse vortices are the second most effective from suppression the separated flow, such as spanwise cylinders, LEBU and elongated arches at +10°angle of attack, Viets' flapper, and transverse grooves. These devices require more complete spanwise coverage resulting in obtaining higher form drag that makes them less effective [54, 56]. The drag reducing riblets have almost no effect on flow separation, whereas the passive porous surfaces and swept grooves examined increase separation. The conventional counter-rotating VGs can efficiently recover the flow from separation. However, they generate highly three-dimensional flow making the vortices too strong downstream. More favourable vortices should be just strong enough to overcome the separation.

Lin et al. [54] indicate that the separation-control effectiveness reduces a little as the VG height decreases from 0.2 to 0.1, but reduces considerably when h/δ is less than 0.1. For many results the device-induced streamwise vortices could last up to100 h but the most effective position of the VGs is between 5h and 30h upstream of the baseline separation [56].

Ashill et al. [58] examined the effectiveness of flow-separation control of Wedge type and counter-rotating delta-vane VGs (SBVGs) over a 2D bump at freestream velocity of 20 m/s. The VGs with h/δ~0.3 (δ~33 mm, e/h~10, Δz/h =12, β=±14) were positioned at 52h upstream of the baseline separation. Even though all VG devices examined depress the separation area, the counter-rotating vanes spaced by 1 h gap seem to be the most effective device in this experiment. It was found that the strength of the device-induced vortices is weaken after 52 h downstream of the device but it still can reduce the effect of the separated flow.

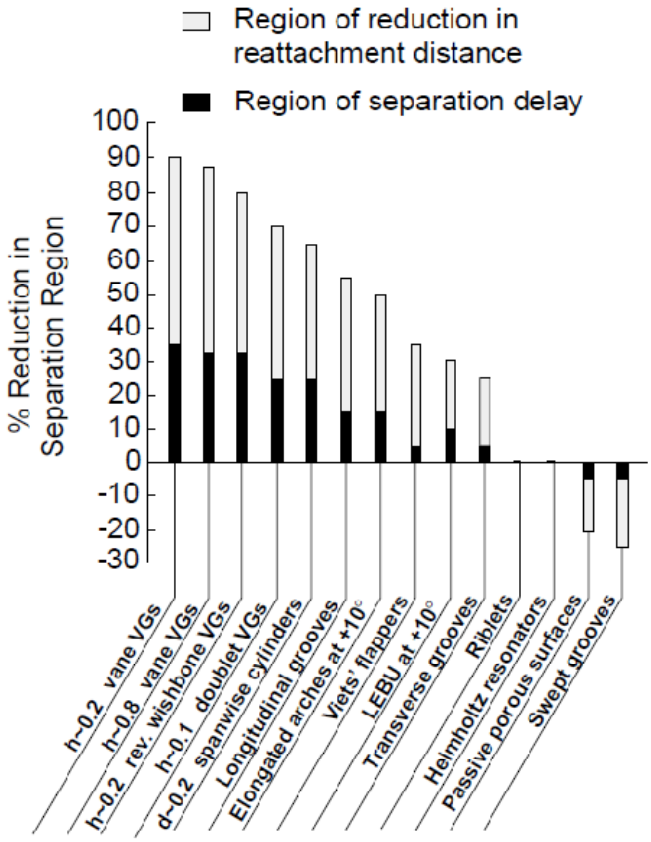

a) Effectiveness in flow separation control V.S. device category

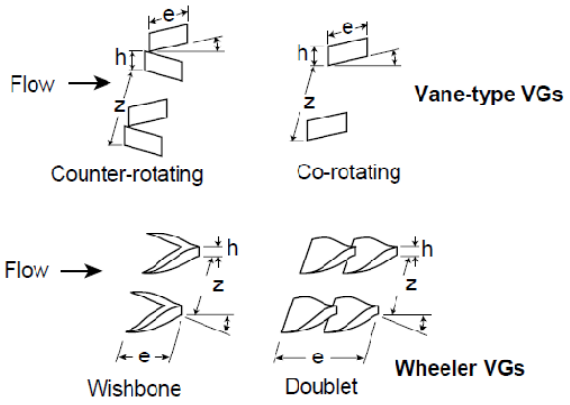

b) VG geometry and device parameters.

Figure 2.4 a) Flow-control effectiveness summary and b) VG geometry [56]

Jenkins et al. [57] conducted another experiment at the NASA Langley Research Center in Low-Turbulence Wind Tunnel at airspeed of 140 ft/s. In the test, two large juncture vortices which occurred each side corner of a backward-facing ramp made the flow to be three-dimensional. The results show that the co-rotating, trapezoidal-shaped, micro-vortex generators with $h/\delta \sim 0.2$ ($e/h = 4$; $\Delta z/h = 4$; $\beta = 23^{\circ}$) effectively reduce the 3D flow separation dominated by the two large vortices.

Many aerofoils are used in low Reynolds number applications, normally less than one million, and encounter a laminar separation bubble before stall. At initial flow laminar boundary layer occurs. This type of boundary layer has low kinetic energy and easy to transition to turbulent boundary layer which has more kinetic energy and is more stable. If static pressure over an aerofoil is high, it may cause the laminar boundary layer to separate from the aerofoil surface. The laminar boundary layer separation causes the separation bubble just downstream of the separation point and the bubble makes an unstable shear layer to rapidly transition to turbulent boundary layer and then the turbulent boundary layer produces reattached flow. Small separation bubbles have little effect on the lift of an aerofoil but they can considerably impact on drag increase due to a thicker turbulent boundary layer. This problem can be solved by reducing the separation bubble resulting in a thinner turbulent boundary layer downstream which could enhance the efficiency of the aerofoil and aircraft.

An experiment on a Liebeck LA2573A low-Reynolds number aerofoil was conducted by Kerho et al. [39] through the use of different submerged vortex generators. The chord Reynolds numbers, Re_c, of the aerofoil examined are between 2 and 5×10^5 at α below the stall angle. The vortex generators were

located at 22% aerofoil chord from the leading edge (after suction pressure peak) in order to control the laminar separation bubble. The VGs produce streamwise vortices that energize the laminar flow near the aerofoil surface to make the adverse pressure gradient less severe; therefore, suppress the laminar separation bubble. Wishbone VGs [31] with h/δ~0.3 (δ~1.6 mm) and ramp cone VGs with h/δ~0.4 are submerged VGs tested and compared with a conventional wishbone VGs (h/δ~0.8). All VGs examined can reduce separation bubble effectively. The smaller heights of the submerged VGs not only provide a smaller profile drag, but their wider spacing also supports device drag reduction more than the larger VGs.

Li-Shu et al. [63] designed Gurney flap and vortex generator attached to WA251A aerofoil to investigate flow control over the aerofoil. The comparisons among cases of study were carried out such as aerodynamic characteristics of clean aerofoil, clean aerofoil with VGs. The triangular VGs used have the height of 4 mm, length of 15 mm, and were attached at 21%c location with three different angles of incidence (15°, 20°, 30°). The application of VGs enhanced the maximum lift coefficient and stall angle, consequently suppressing the flow separation. These VGs produce longitudinal vortices, which energize the boundary layer to tolerate adverse pressure gradient for delaying the flow to separate from the aerofoil surface. As a result drag is reduced after the stall. For the angles of incidence the 15° to the free stream flow VG has better performance than the 20° and 30°. The Gurney flaps (GFs) do not only greatly increase the lift but also increase the drag of the aerofoil for all angles of attack. The combination between the VG and GF not only gives higher lift enhancement than each device individually but also gives more drag than only VG configuration so the advantages of VG over GF and GF&VG configuration are lower drag for all regimes of operation and easier to employ to aircraft wings.

Godard and Stanislas [64] made a 2D geometry to mimic adverse pressure gradient on the section side of an aerofoil by modelling a bump in boundary wind tunnel to characterize the separation flow in a correlated project called AEROMEMS. Hot film shear stress probes were employed to measure skin friction to optimise the flow with passive VGs. Hot wire anemometry and PIV are instruments used to characterize the flow. There were two types of VGs tested: Co-rotating VG and Counter-rotating VG. The co-rotating vortices caused by co-rotating VG array transport low momentum air away from the surface and higher momentum approach the surface between two adjacent streamwise vortices as illustrated in Figure 2.5(a). For counter-rotating VG, the low momentum is transported upward between two different VGs,

whereas the high momentum is transported downward to the surface around the plane of symmetry of each pair of VGs as shown in Figure 2.5(b).

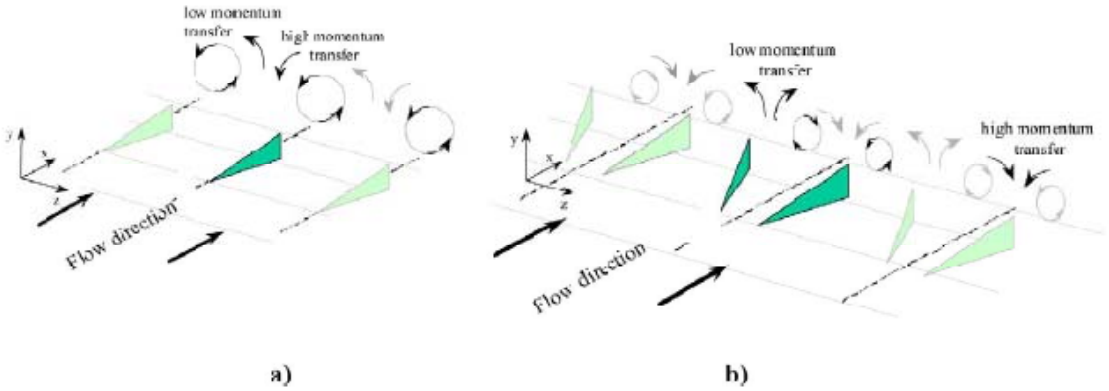

Figure 2.5 Configurations of (a) Co-rotating VGs. (b) Counter-rotating VGs. [64]

The counter-rotating VGs can keep an array of vortices near the surface in adverse pressure gradient far downstream and are effective for distances of 17-52 times of the streamwise distance between the device and the minimum skin friction line. Results show that triangular VGs produce higher lift and lower drag than rectangular one. The PIV results based on the counter-rotating vortices in Figure 2.6 illustrate the flow structure showing the way momentum transfers between the near wall zone and the outer flow. While the vortices go downstream, they grow rapidly in size and remain attached to the surface.

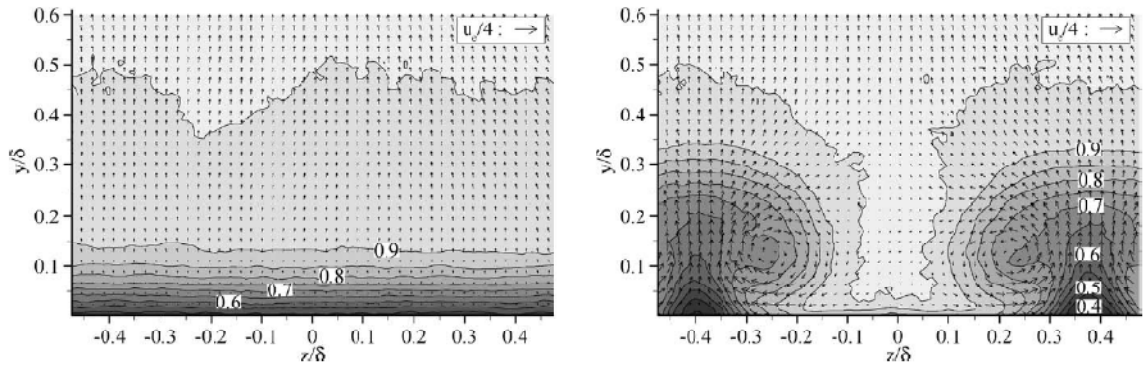

Figure 2.6 Mean velocity maps at ΔX/h =22, for the smooth wall and counter-rotating VG. The vectors show velocity components in y-z plane [64]

Velte et al [71] executed stereoscopic particle image velocimetry (SPIV) measurements in a low speed wind tunnel with low Reynolds number (20,000) to investigate the effect of vortex generators in turbulent separated flow. The measurement technique provides three velocity components in

four spanwise planes where the flow moves past a row of counter-rotating vortex generators, attached on a bump. The results show that the mean velocity field for uncontrolled case acts like 2D boundary layer, encountering separation close to the bump trailing edge. The VGs, controlled case, causes counter-rotating streamwise vortices, exchanging high-momentum flow from the outer flow with low-momentum flow near the wall in the downwash region. The results also shows that the longitudinal vortices do not move considerably in the spanwise direction.

Nickerson [65] utilized NACA0024 aerofoil to test co-rotating vane-type vortex generators at chord Reynolds number of 100,000, 150,000, and 200,000. The VGs were located at 5% and 7.5% of the chord. Dimension of the VGs were 1.016 cm high by 0.381 cm long with a 45° degree slope tip to reduce drag. Over Reynolds number regime tested, it was found that the use of VGs was advantageous compared to the aerofoil with no VGs due to stall angle increment. The VGs attached to the surface at 5% chord position has better performance than that at 7.5% chord position.

Fernández-Gámiz U. et al. [66] investigated the vortex path variation produced by a rectangular VG mounted on a flat plate. Five VGs with different height ($h_4 = 0.2\delta$, $h_3 = 0.4\delta$, $h_2 = 0.6\delta$, $h_1 = 0.8\delta$ and $h = \delta$) were simulated at Re= 1,350 based on the conventional VG height of 0.25m with an angle of incidence 18.5°. The simulation was carried out by the implementation of RANS equations using QUICK scheme and k-ω SST turbulence model. Three parameters were used to identify vortex development: peak streamwise vorticity $|\omega_x|_{max}$, vortex circulation Γ and vortex core location. Results show the vortex development up to the position 15δ downstream the VGs. Figure 2.7 exposes the vortex paths generated by the conventional VG (h) and the low-profile VGs (h_1,h_2,h_3, and h_4). If the position of the vortex core respect to downstream distance(x) is known, one can find the paths of the vortex in both y (lateral) and z (vertical) directions. The x coordinates are dimensionless by the local boundary layer thickness and the y and z coordinates are dimensionless by the corresponding VG height. The vortex from the lowest VG, h_4, has the smallest deviation in y direction but has the highest deviation in z direction compared to the others. The vortex from h_4 behaves very differently from the others as moving far away from the VG. This may be because the vortex generated by the lowest VG is under the inner part of the boundary layer where the viscous shear dominates so that strong interaction between the vortex and the wall occurs. This influence is explained by inner law pointed out by Prandtl in 1933.

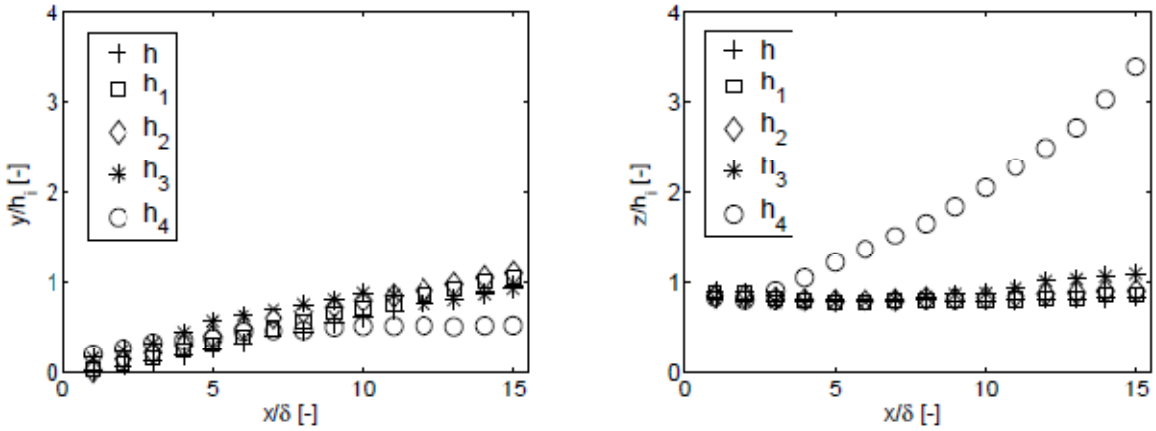

(a) Non-dimensional lateral path (b) Non-dimensional vertical path

Figure 2.7 Effect of VG size on vortex core trajectory [66]

Normalised peak vorticity is plotted as a function of non-dimensional downstream distance x/δ for all cases. Figure 2.8(a) indicates that the vortices rapidly decay downstream of the VG for all cases. The peak vorticity decays exponentially and inversely proportional to x/δ. The peak vorticity depends on the height of the VG. While the height is increased, the peak vorticity increases. An indicator used to quantify the strength of the vortices is the positive circulation, Γ^+. This can be calculated by equation (1), which is the integration of the peak vorticity over the area surrounding the vortex core in cross-flow plane normal to the wall.

$$\Gamma^+ = \int_s \omega_x^+ \, ds \qquad (1)$$

Figure 2.8(b) shows the relation of the non-dimensional positive circulation as well as streamwise distance locations. The non-dimensional positive circulation is nearly independent of the VG height except h_4. The non-dimensional circulation of h_4 decreases after reaching its maximum value at x/δ =4 because of viscous dissipation and reduce to zero at position far away from the VG. The reason that h_4 differs from the others because the VGs are in the inner part of the boundary layer as stated before. Therefore the thin layer close to the wall is dominated by viscous effect.

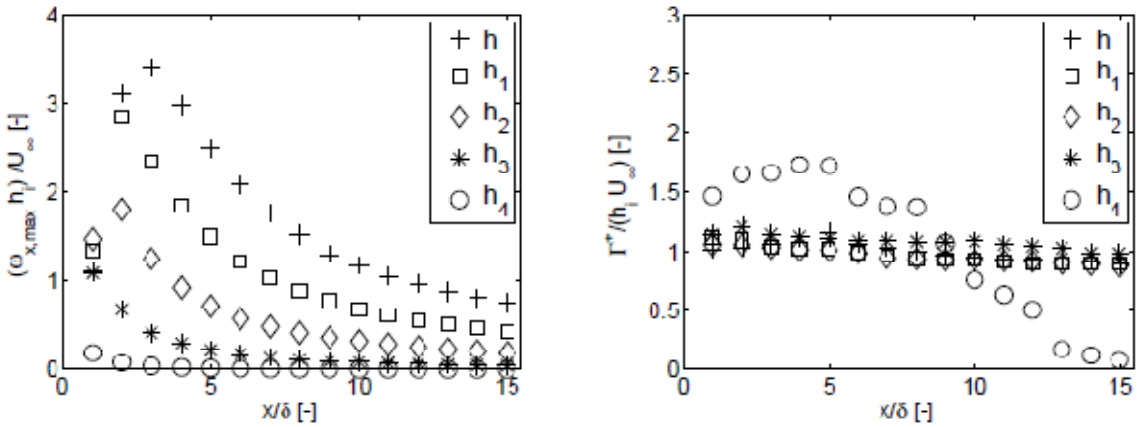

(a) Non-dimensional streamwise peak vorticity

(b) Non-dimensional positive circulation

Figure 2.8 Effect of VG size on vortex decay and vortex strength [66]

Angele and Muhammad [67] investigated high Reynolds number turbulent boundary layer on a flat plate subjected to an adverse pressure gradient. Means of streamwise vortices to control a separating adverse pressure gradient was employed and PIV measurement was used to visualize mean flow and turbulence structure. The experiment show that viscous diffusion results in the growing vortices, decreasing swirling velocity component and two-dimensional state boundary layer development. The counter-rotating streamwise vortices changes from non-equidistant to equidistant and are still in the boundary layer.

U. Anand et al [68] carried out numerical simulations of turbulent flow on a NACA0012 aerofoil attached with counter-rotating VG at Reynolds number of 550,000. Spalart-Allmaras (SA) turbulence model was selected to model the effect of turbulent Reynolds stress terms in momentum equations due to more stable and less sensitive to the grid solution than two-equation models and work well with adverse pressure gradient and separation. At 11° attack angle the streamlines of aerofoil with and without VG are almost the same. The flow is attached over the upper surface and makes aerodynamic force coefficients a bit different. At 14° the clean aerofoil starts to stall but the VGs help to postpone the stall of the aerofoil to the higher angle of attack (16°). The disadvantage of the VGs is that it generates higher drag at a low angle of attack with both skin friction and induced drag. At a higher angle of attack with separation flow pressure drag greatly influences total drag so the VGs decrease pressure drag resulting in lower total drag.

Delnero et al [69] used a low Reynolds number aerofoil Eppler 387 (42cm chord and 80cm span) on which triangular vortex generators were placed to

determine aerodynamic characteristics by using force balance and flow visualization systems. The VGs are 40mm long, 10mm high and 0.5mm thick. These passive VGs were placed as counter-rotating vanes but no detail how close they are for each pair of the VGs. The VGs were tested with different positions from the leading edge of the aerofoil (10%c and 20%c) and different angles of incidence of VGs (0°, 10° and 20°) at the airspeed of about 8 m/s (Re = 300,000). When using the VGs with various incidence angles of the VGs at both positions, maximum lift coefficient increases compared to the clean configuration aerofoil, whereas stall angles of attack have a little change. This tendency could be explained in that the lift enhances because the VGs produce spiral vortex interacting with the boundary layer and modifying the flow characteristics behind the devices so that the incidental flow sees the thickness of the aerofoil larger. At low angles of attack regime, the drag coefficient of the clean aerofoil is a bit lower than that of the aerofoil with the VGs. As the angle of attack increases, the drag dramatically increases, especially at higher incidence of the VGs. This increment is due to the interaction between the vortices generated and the boundary layer.

H. Tebbiche and M. S. Boutoudj [70] studied the flow control using a new counter-rotating VGs. The VGs were attached at 10% from the leading edge on the upper surface of NACA0015 aerofoil. An experimental design method [44] is used for optimizing the geometry of the VGs. The experiments were conducted in a DeltaLab type open circuit subsonic wind tunnel at Reynolds numbers of 158,000 and 260,000. At the higher Reynolds number, the VGs are more effective by increasing 14% of maximum lift coefficient, whereas maximum lift coefficient increases 5% in case of lower Reynolds number. In addition, the VGs increase stall angle by 2º for both cases. For the efficiency of the VGs on drag reduction, drag decreases around 16% at lower Reynolds number and 11% at higher Reynolds number.

Sorensen et al [72] applied a CFD method to two different aerofoils, FFA-W3-301 and FFA-W3-360, at Reynolds number of 3 million to predict the aerodynamic characteristics and then compare one with the experimental results. The DTU Wind Energy flow solver EllipSys3D was used for the computations. The turbulence model k-ω Shear Stress Transport (SST) eddy viscosity was used to model the flow. The VGs used are triangular counter-rotating VGs. For all cases the VG height (h) is 1 percent of the chord length, the aspect ratio (l/h) is 3.8, the incoming flow angle is 15.5 degrees, the distance between the same pairs is 5h at the leading edge of the VG, and the distance between the different pairs is 9h at the leading edge. The VGs were placed at three different positions having x/c = 0.15, x/c = 0.2 and x/c = 0.3. The computational data were compared to the experimental data taken in

Stuttgart Laminar Wind Tunnel. A delay in stall angle can be observed by a decreasing lift slope close to stall as moving the VG towards the leading edge. A penalty of using VGs is an increase in drag at low angle of attack due to more skin friction and induced drag caused by the VG. The FFA-W3-360 aerofoil tested has results similar to that of the FFA-W3-301 aerofoil.

2.3 Boundary layer trips (BLTs)

Lissaman [88] indicated that aerofoil performance is quite poor at Reynolds numbers lower than 70,000. However, at low Reynolds numbers between 70,000 and 500,000, the aerofoil performance can be enhanced by adding some devices to make transition faster. This process energizes the boundary layer and so prevents flow separation. Many devices can be utilized including boundary layer trips (wires, tape strips, grit, tube or rod), surface suction or blowing, synthetic jets and vortex generators. Although the boundary layer trips may not lead to performance improvement and can result in some losses, it is a good try to do some boundary layer trip experiments to determine the phenomena and characteristic of such flow.

Huber II and Mueller [85] investigated the performance and boundary layer characteristics of the Wortmann FX 63-137 aerofoil with and without trip wire roughness. Data were gathered through a three-component strain gage force balance and pressure gage at chord Reynolds number of 100,000. They used equations 2.1 and 2.2 to determine roughness height (k) as required at a certain location on the aerofoil. This equation has been used in case of a flat plate but it is a good try to be used to an aerofoil. Experimental data show that separation with a formation of laminar separation bubbles greatly affects the aerofoil's performance. The effects of the additional trip wire roughness to the aerofoil performance depend on location and height. The trip wire located on the upper surface can considerably reduce $C_{l\max}$ and $(C_l^{3/2}/Cd)_{max}$ while improving or degrading $(C_l/C_d)_{max}$ depending on the roughness height. Trip wire roughness height located near the point of maximum thickness can reduce $C_{d\,min}$ and also improve the maximum lift to drag ratio.

$$k = \frac{826\nu}{U_e}\exp\left(-0.9\Lambda_1\right) \tag{2.1}$$

$$\Lambda_1 = \frac{\delta_1^2}{\nu}\frac{dU_e}{ds} \tag{2.2}$$

Vera et al [81] have presented the effect of a single spanwise two-dimensional wire on the downstream position of the boundary layer transition under steady and unsteady inflow conditions. The work was conducted by using high turning, high-speed, low pressure turbine (LPT) blade (40 mm chord) in

a transonic wind tunnel. The results show that the use of a trip wire reduces the profile losses up to Mach number of 0.8 both steady and unsteady inflow conditions.

Howell and Roman [80] investigated the use of roughness elements (distributed roughness, distributed roughness recessed, a wire, a steps) and their location on the blade surface and wake unsteadiness to reduce the profile losses generated on two different types ultra high lift low pressure turbine blade; ultra high lift(UHL) and extended ultra high lift(XUHL). Measurements were taken at Reynolds numbers ranging from between 100,000 and 210,000. Results show that distributed roughness decreases the size of the separation bubble with steady flow. The distributed roughness amplified disturbances in the boundary layer making the transition take place, thus the separation bubble was eliminated. The extended ultra high lift profile gave slightly higher loses than the ultra high lift profile but produced 12% greater lift and 25% more diffusion. The experiments show that roughness element located inside the separation bubble had less effect on reducing losses than one located upstream of the separation point. The optimum roughness element for loss reduction of this investigation is distributed roughness aluminium oxide grains R120 (100μm in height) located at 50-60%S with wake unsteadiness, which reduce the length of the separation bubble on the XUHL profile by half. Relative loss of various roughness elements is shown in Figure 2.9.

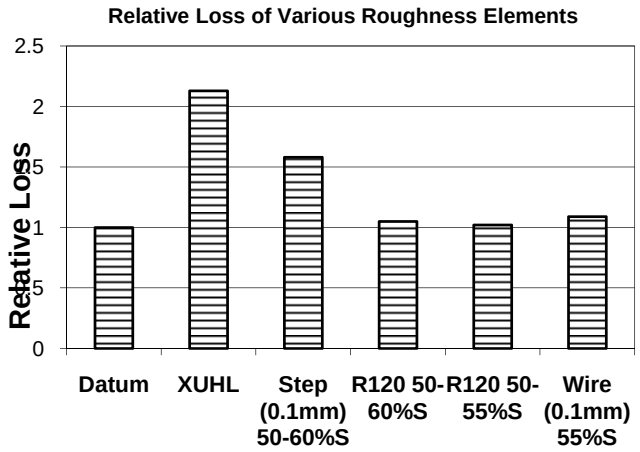

Figure2.9 Relative loss generated by UHL and XUHL profiles, reduced frequency of 0.38 at Re = 130,000 [80]

Lyon et al [79] investigated three types of boundary layer trips (single 2D plain, multiple 2D plain, and 3D trips) on the M06-13-128, E374, and SD7037

aerofoils over the Reynolds number of 100,000 to 300,000. Trip locations on the three aerofoils are shown in Figure 2.10. The first trip was located at 0.1 in upstream of the predicted bubble. The next trip was located at 1 in. further upstream along the aerofoil chord surface and so on.

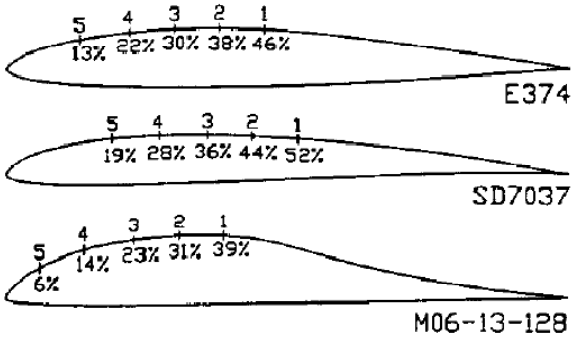

Figure 2.10 Trip locations on the three aerofoils [79]

The single 2D trips were a rectangular tape strip. Figures 2.11a and 2.11b show data conducted on the M06-13-128 for several trip heights and locations. Trip1 was submerged within the laminar separation bubble. Therefore, it produced little effect on the total drag. It was observed that for Re= 300,000, drag reduced in the range of the heights between 0.026 and 0.03 in. This may be because the trip protruded through the separation streamline of the bubble, making the bubble shorten. At location 3, drag dramatically reduced for both Reynolds numbers and trip heights. While the trip height was increased, the total drag decreased due to the reduction in the size of the bubble, which had greater effect than increased device drag. It is suggested that at higher Reynolds number, the optimum trip heights become smaller. The effect of single trips on the E374 was investigated at points 1, 3, and 5 at various Reynolds numbers. The tendencies of the results are very similar to that of the M06-13-128 aerofoil. The decrease in drag occurred as the trip was moved forward and out of the bubble.

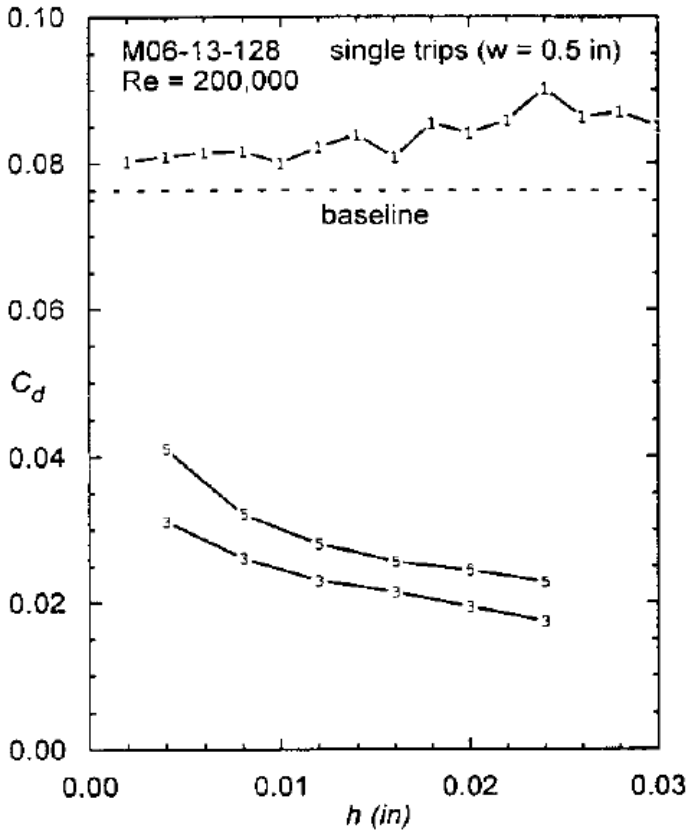

(a)

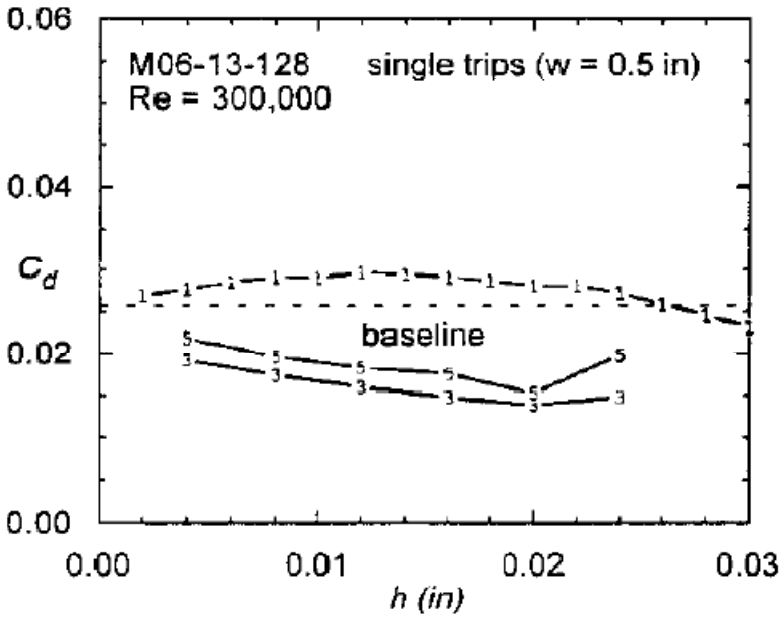

(b)

Figure 2.11a, b Drag data for single 2D plain trips with various thicknesses [79]

For multiple trips, they consisted of several plain trips placed together at adjacent locations. Figures 2.12a and 2.12b show the results obtained for the aerofoil M06-13-128 at Re=200,000 and 300,000 respectively. When comparing between single 2D trip and multiple 2D trip, it was found that the three multiple trip, 3M (located at points 1-3) had slightly lower drag over the trip heights tested. This implies that increased device drag from multiple trips was compensated by increased flow disturbances leading to reduced bubble drag.

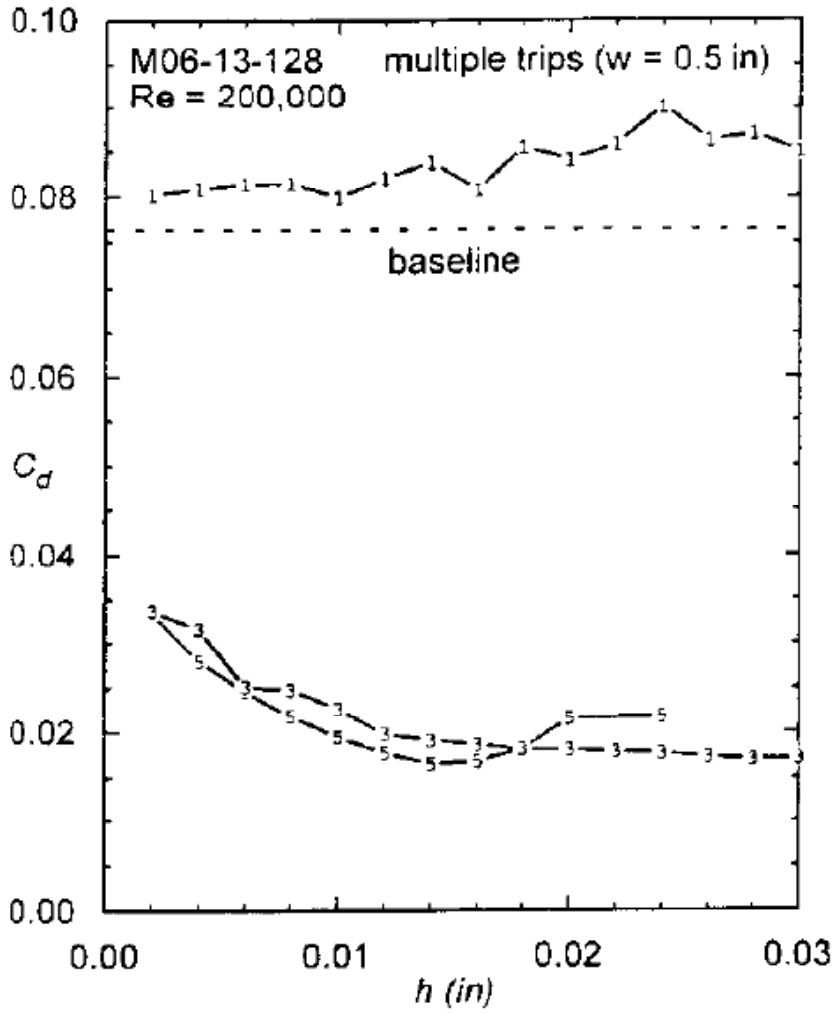

(a)

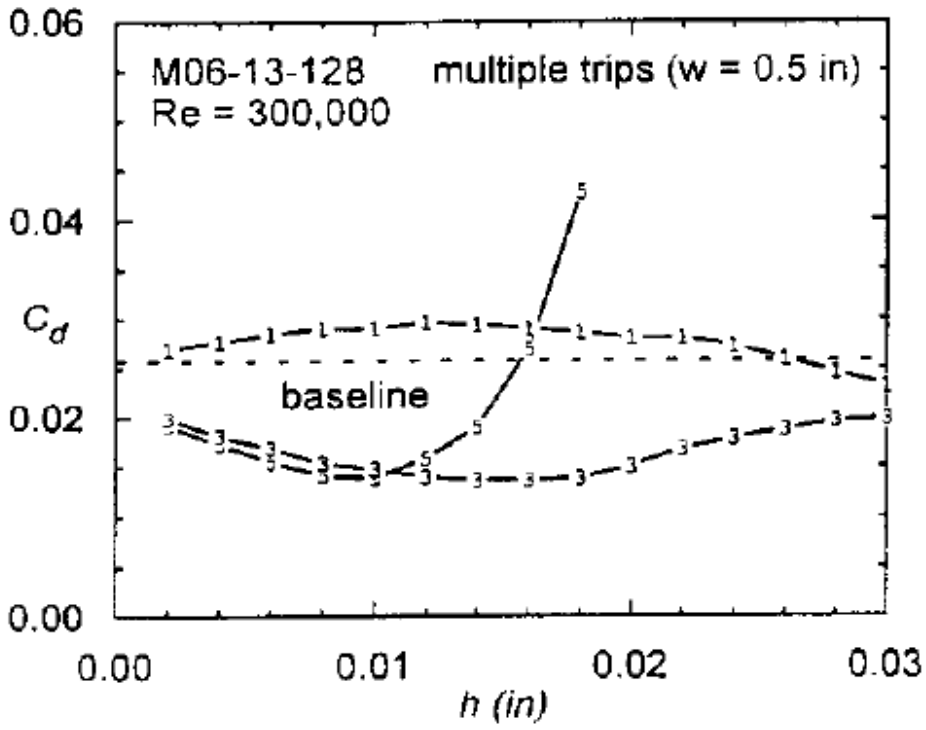

(b)

Figures 2.12a, b Drag data for multiple 2D plain trips of various thicknesses [79]

For multiple trips tested on the E374, usually, as the number of trips was increased, the drag was reduced at all Reynolds numbers, especially at Reynolds number of 100,000 where maximum drag reduction occurred for multiple trips 5M (located from points 1 to 5) at h= 0.014 in.

Several types of 3D trips were tested on the E374 at a Reynolds number of 200,000. These are triangular patches (Hama trips), conventional zigzag, crescent zigzag, and raised hemisphere trips. Figure 2.13 shows the drag produced by each configuration. From the Figure 2.13, it was found that the bigger configurations perform better than the smaller ones.

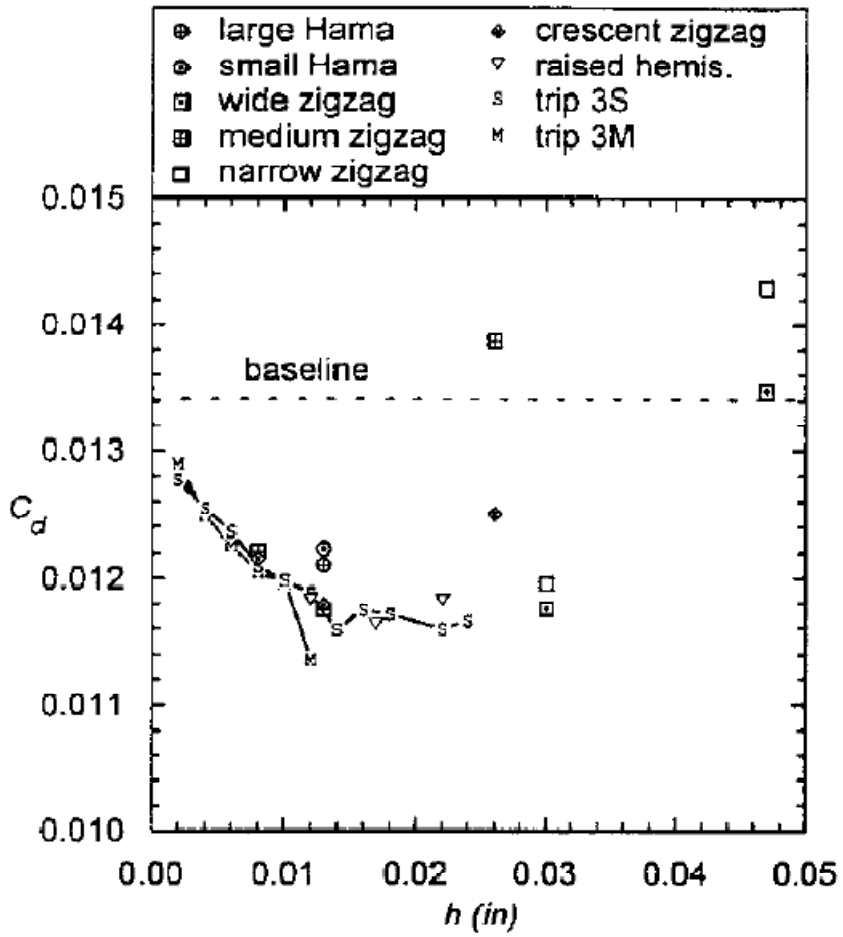

Figure 2.13 Drag data of E374 for 3D trips of various thicknesses at Re=200,000 [79]

All experiments have shown that aerofoils with large laminar separation bubbles obtained the most benefit from using boundary layer trips. No trip configuration generated lower drag than a clean aerofoil with low bubble drag.

Philippe and Michael [82] conducted wind tunnel experiments to investigate the effects of leading edge tape used on small wind turbines, which is used to prevent blade erosion. Lift and drag were measured over the Reynolds numbers from 150,000 to 500,000 on five aerofoils which are the BW-3, FX 63-137, S822, SG6042 and SG6051. The tape edge was positioned at either 5%, 15%, or 30% on the suction and pressure surface. The results have shown that the transition was stimulated early and the separated laminar boundary layer transition to turbulent flow effecting on drag. The drag depended on the net of summation among bubble, device and skin friction drag. The results of the five aerofoils tested with one-layer tape for overall effects on lift are small. For two-layer tape, the lift curve slope slightly decreased. The drag polars for the SG6042 aerofoil with one-layer tape was considerably

reduced at a Re of 150,000 because the laminar separation bubble dominated the flow, whereas the effect decreased as the Reynolds numbers increased. Therefore, at higher Reynolds numbers, especially at Re=500,000, the bubble drag reduced but device and skin friction drag increased. All of the results indicated that the ending of the tape should be extended up to 15%-30% chord to avoid aerofoil performance being reduced.

Kwangmin et al [83] investigated the effect of a trip wire on the flow around a sphere. The experiments were conducted at Reynolds numbers between 50,000 and 280,000 based on sphere diameter at different points on the sphere surface (20°-70° from the stagnation point) and different diameters of the trip wires ($0.33x10^{-2} < k/d < 1.33x10^{-2}$). Figure 2.14 shows the mechanism of drag reduction by the surface trip wire where $k/d = 0.33x10^{-2}$. The drag is not reduced at low Reynolds numbers, although the trip induces the disturbance to the downstream. At moderate Reynolds numbers, the disturbance occurred from the trip wire decays downstream but effective enough to delay the separation. At high Reynolds numbers, the disturbance produced by the trip wire stimulates the laminar boundary layer transition to the turbulent boundary layer resulting in delaying the separation. Nevertheless, if the trip wire is much larger than the local boundary layer thickness and the Reynolds number is not large enough, the reattached flow behind the trip will not bring enough near-wall momentum so drag reduction does not occur. On the other hand, if the flow has large Reynolds numbers, this will cause a dramatic decrease in drag.

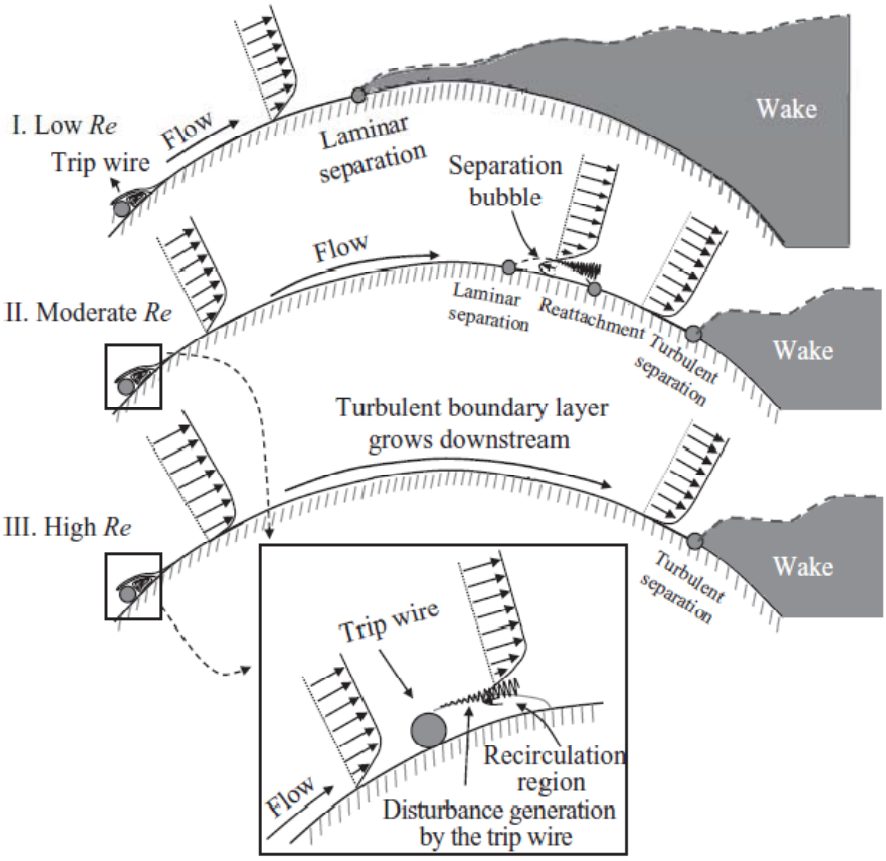

Figure 2.14 Mechanism of drag reduction by the trip wire [83]

Wong et al [84] studied the effectiveness of the burst control plate attached at different locations (5%, 7.5% and 10% of an aerofoil chord) on a NACA 63_1-012 aerofoil section for laminar separation burst delay and aerodynamic characteristics improvement at a chord Reynolds number of 130,000. The parameters for control the effectiveness of the burst control are the height, width of the plate and the position of the trailing edge of the plate. The experimental results have shown that when the plate height (h/c) is increased from 0.005 to 0.0075, the stall angle of the aerofoil is also increased for both types of the plates (thin and rectangular plates). The maximum lift coefficient was increased for all cases tested. It is recommended that the plate should be placed ahead of the flow reattachment point and the leading edge height of the plate should be the same level as the height of the separated shear layer. At the angle of attack greater than 9°, the lift generated is considerably higher than that of the clean aerofoil as shown in Figure 2.15, whereas the drag is sufficiently decreased as shown in Figure 2.16. The overall results proved that the application of the burst control plate can be implemented as an effective

method in controlling the bubble and delaying the aerofoil stall at low Reynolds numbers.

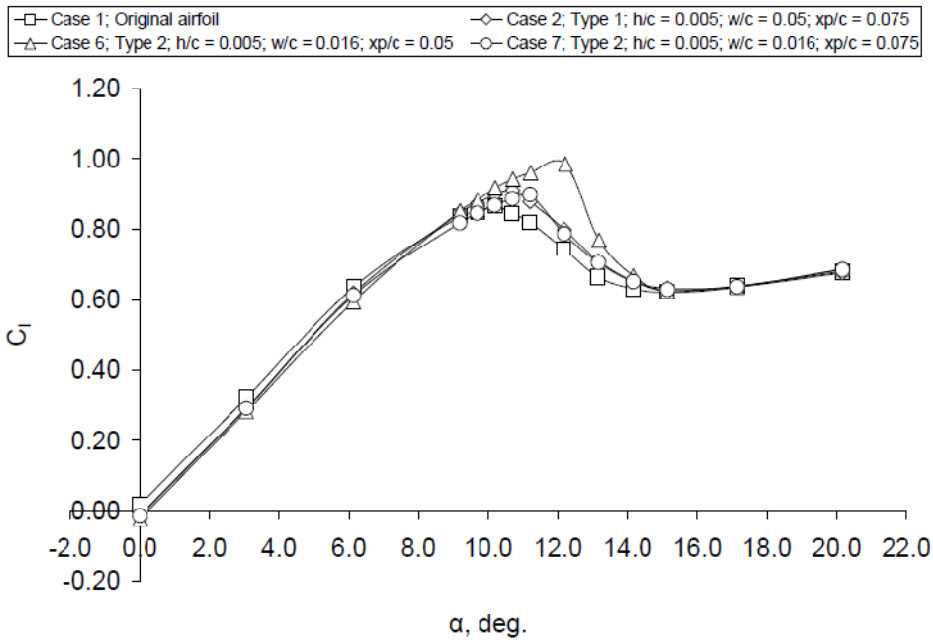

Figure 2.15 Lift coefficients for different cases [84]

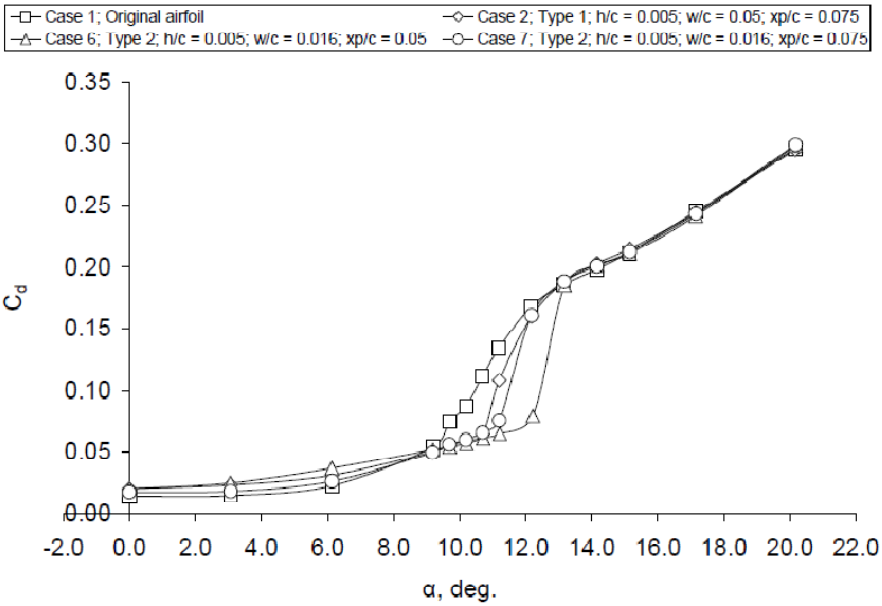

Figure 2.16 Drag coefficients for different cases [84]

Erm et al [86] investigated a method used to match the size of a circular wire tripping device with the freestream velocity to get the correct turbulent boundary layers needed on a body of revolution. The circular wires had diameters of 0.1, 0.2 and 0.5 mm and were glued to the model around its

circumference at a distance of 67.4 mm from the nose (5% of the model length). Turbulent skin-friction coefficients were measured along the model for the velocities from 40m/s to 70m/s. The results were found that a wire diameter of 0.2 mm was the best wire size to trip the boundary layer for the tests.

There are many useful methods that can be implemented in order to improve the flow to prevent, delay or suppress the boundary layer separation. This thesis firstly focused on synthetic jets and vortex generators but due to time constraints, the objective has been changed to the study of the boundary layer trips. Although the method has been changed, some concepts can be used as a guide. The investigation of the effect of the boundary layer trips with different sizes of circular tubes and different locations on a NACA 0015 aerofoil wing was conducted at a low Reynolds number of 78,000 in subsonic wind tunnel at Mechanical engineering department, the University of Sheffield. The concept is to reduce the size of the laminar separation bubbles by means of disturbance the flow with the trips resulting in bubble drag reduction.

3. Theory

3.1 Aerodynamic forces and moments

The generation of aerodynamic forces and moments on bodies immersed in air are due to only two basic sources which are: Pressure distribution and Shear stress distribution over the body surface [29]. Pressure acts normal to the surface and shear stress, which is caused by friction between the body and the air, acts tangential to the surface.

The effect of pressure (p) and shear stress (τ) is a resultant force and moment on the body. The resultant force can be split into components as shown in Figure 3.1. V_∞ is called relative wind, defined as the flow velocity far ahead of the body. It is also called free stream velocity. The chord c is the linear distance from the leading edge to the trailing edge of the body. By definition,

L = lift = component of R perpendicular to V_∞

D = drag = component of R parallel to V_∞

N = normal force = component of R perpendicular to c

A = axial force = component of R parallel to c

α = angle of attack = the angle between V_∞ and c, D and A, and L and N

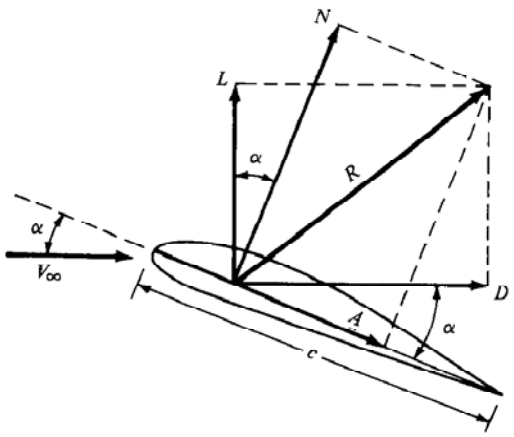

Figure 3.1 Resultant aerodynamic force and the components into which it splits [29]

The lift and drag can be determined from the normal force and axial force by applying the equations below:

$$L = N\cos\propto -Asin\propto$$
$$D = Nsin\propto +Acos\propto$$

The dimensionless force and moment coefficients are quantities of more fundamental use than the aerodynamic forces and moments because they can be used to compare aerodynamic characteristics of any size of bodies, defined as follows:

Lift coefficient: $C_L \equiv \frac{L}{q_\infty S}$

Drag coefficient: $C_D \equiv \frac{D}{q_\infty S}$

Normal force coefficient: $C_N \equiv \frac{N}{q_\infty S}$

Axial force coefficient: $C_A \equiv \frac{A}{q_\infty S}$

Moment coefficient: $C_M \equiv \frac{M}{q_\infty S l}$

$q_\infty \equiv dynamic\ pressure \equiv \frac{1}{2}\rho V^2$

$s \equiv reference\ area$

$l \equiv reference\ length$

Two additional dimensionless quantities are

Pressure coefficient: $C_p \equiv \frac{p-p_\infty}{q_\infty}$

Skin friction coefficient: $C_f \equiv \frac{\tau}{q_\infty}$

For experiments, the normal and axial force acting on a body can be measured by use of a force balance. When these values are known the lift and drag coefficients can be obtained.

From dimensional analysis the factors affecting the aerodynamic forces and moments for a given body shape in subsonic flow regime are Reynolds number, Mach number and angle of attack.

3.2 Downwash and induced drag

An aerofoil is considered as part of a two-dimensional infinite wing. This makes the flow two-dimensional so that the aerodynamic characteristics differ from a three-dimensional wing, known as a finite wing. For a 3D wing the pressure difference between the upper surface and lower surface makes the flow around the wing tips to curl around the tips, being forced from the high pressure region just underneath the tips to the low pressure region on top, as shown in Figure 3.2 [29].

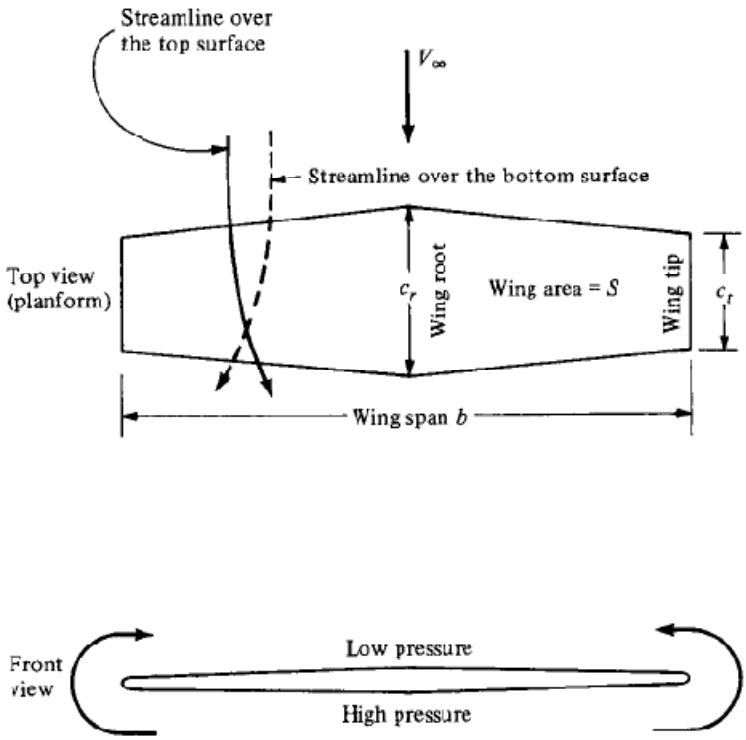

Figure 3.2 Finite wing three-dimensional flow [29]

As a result, there is a spanwise flow from the tip towards the wing root on the top surface of the wing, whereas there is a spanwise flow from the root towards the wing tip on the bottom surface. The flows at the wing tips are called wing-tip vortices, as shown in Figure 3.3 [29].

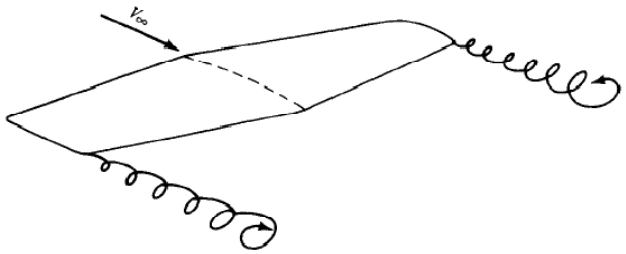

Figure 3.3 Schematic of wing-tip vortices [29]

The wing-tip vortices downstream of the wing induce a small downward component of air velocity called downwash. This downwash reduces the angle of attack, moreover, generates a component of drag called induced drag as a result of the downwash tilts the lift force vector backward, as shown in Figure 3.4. This results in lift lose and drag increase, so the lift and drag coefficients at the same conditions for the finite wing differ from that for the infinite wing or aerofoil section. Some correction is needed to correct the results from the 2D wing to the 3D wing.

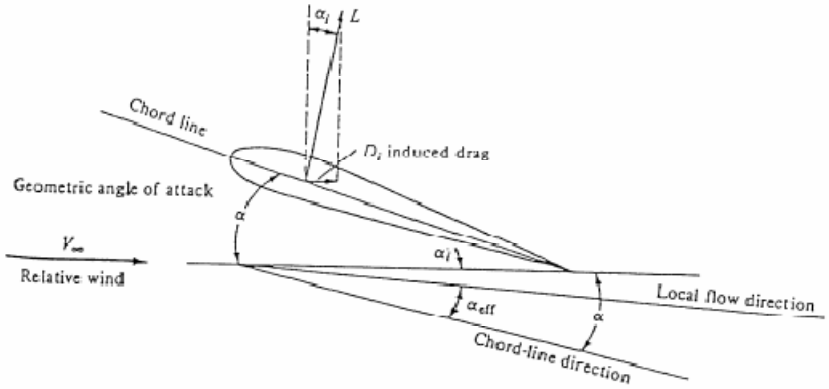

Figure 3.4 Induced drag and lift components

3.3 Finite wing correction

All real wings are finite in span making the lift coefficient of a wing different from that of an aerofoil as mentioned before. The correction can be done to obtain lift curve slope for a wing from an aerofoil if the aspect ratio of the wing and lift curve slope of the aerofoil are known.

For a high-aspect-ratio straight wing (incompressible and AR≥4), by applying Prandtl's lifting line theory, the lift curve slope for a finite wing can be determined.

$$a = \frac{a_0}{1+\frac{a_0}{\pi e AR}}$$

For a low-aspect-ratio straight wing (incompressible and AR<4), by applying Helmbold's equation, the lift curve slope for a finite wing can be determined. This equation was used to correct the lift curve slope of an NACA 0015 aerofoil as that of the NACA 0015 aerofoil wing with AR = 3.5 in Chapter 5.

$$a = \frac{a_0}{\sqrt{1+(\frac{a_0}{\pi AR})^2}+\frac{a_0}{\pi AR}}$$

Where;

a = lift slope for a finite wing
a_0= lift slope for a 2D wing
AR = aspect ratio of a wing = $\frac{b^2}{S}$
b = wing span
S = wing surface area

3.4 Flow separation

The typical variation of lift coefficient with angle of attack for an aerofoil is shown in Figure 3.5.

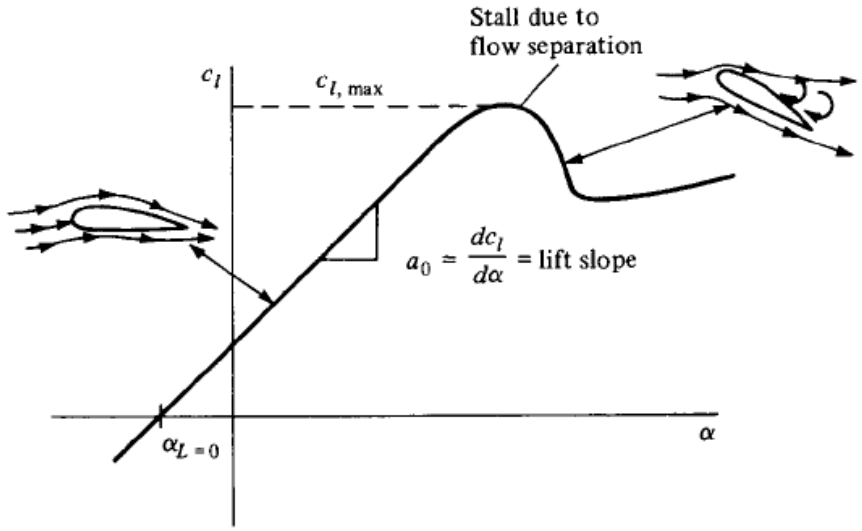

Figure 3.5 Schematic of lift-coefficient variation with angle of attack for an aerofoil [29]

Lift coefficient varies linearly with the angle of attack between low and moderate angle of attack (AoA) and the flow is attached over most of the surface. In this region, the flow moves smoothly over the aerofoil. Nevertheless, as AoA is large, the flow tends to separate from the top surface of the aerofoil, creating a large wake behind the aerofoil as shown in Figure 3.5. This separated flow is due to viscous effects and resulting in a decrease in lift and a huge increase in drag.This condition is said to be stalled. Many methods are used to improve the flow around the aerofoil in order to delay or alleviate the stall. These include synthetic jets and vortex generators. To better understand the physicals of flow separation, more explanation is given.

For all Reynolds numbers of fluid flows there is a thin region close to the wall where it is affected by viscosity. This region is called boundary layer and the specific behaviour of this layer can make the flow to separate. Pressure distribution over a surface can result in the boundary layer development. If the pressure decreases downstream, this will make the boundary layer attach to the wall. Nevertheless, if the pressure starts to increase downstream of the flow, so-called adverse pressure gradient, this may result in the boundary-layer separation. Prandtl explained that when the velocity in the boundary layer drops towards the wall, the kinetic energy of fluid

particles inside the layer also drops towards the wall until it is zero at the wall. This means that if the adverse pressure gradient is strong enough, the fluid particles near the wall will stop moving and could turn back to upstream direction forming a recirculating flow region characteristic of separated flows.

The boundary layer velocity profile development in an adverse pressure gradient area of a flow over the wall is presented in Figure 3.6. The velocity gradient, $\partial u/\partial y$, is positive upstream of separation but it is zero at the separation point and negative in the reverse flow area. Downstream of the separation point it is possible for the shear layer to reattach to the wall surface or form a wake and not to reattach to the surface again.

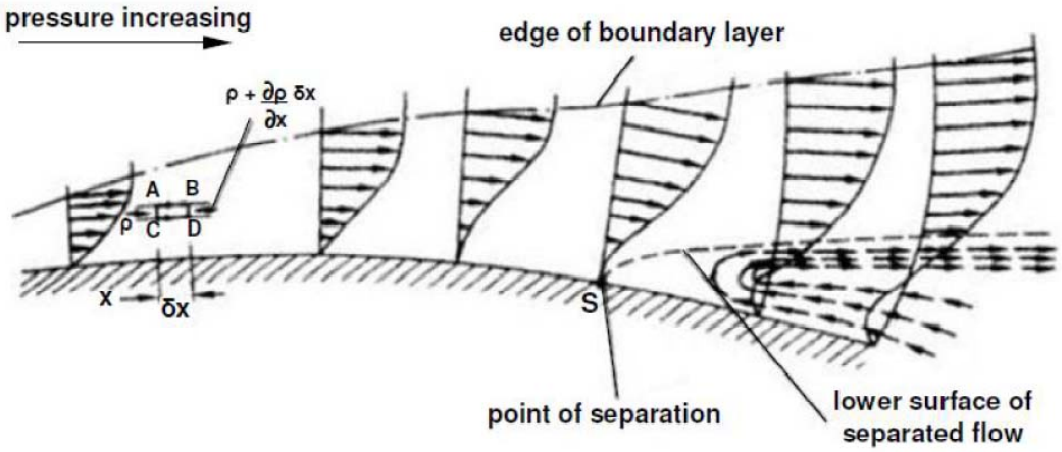

Figure 3.6 Separated flow region in an adverse pressure gradient

3.5 Boundary layer transition

There are two types of boundary layer: laminar and turbulent. The flow is initially the laminar boundary layer and then with factors it transfers to the turbulent boundary layer. The laminar-turbulent transition in air stream on a flat plate with sharp leading edge at zero incidence takes place at a point where the Reynolds number is between 3.5×10^5 to 10^6 [9]

The Tollmien-Schilichting (T-S) instability transition mechanism is used to explain the phenomena of subsonic boundary layers, apart from swept wing where cross-flow instability is important. For two-dimensional zero pressure gradient boundary layer, the process can be summarized as shown in Figure 3.7. Above the indifference Reynolds number(Re_{ind}) the laminar boundary layer becomes sensitive to small disturbances, leading to amplification of

unstable two-dimensional linear T-S waves (primary instability). Once these primary T-S waves exceed a threshold value of 1% of the freestream velocity [90] they slowly become three-dimensional and form hairpin vortices (non-linear secondary instability). These then interact together and are intensified as they are stretched to form the turbulent spots. The turbulent spots grow as they propagate downstream and they eventually merge, leading to a fully turbulent flow.

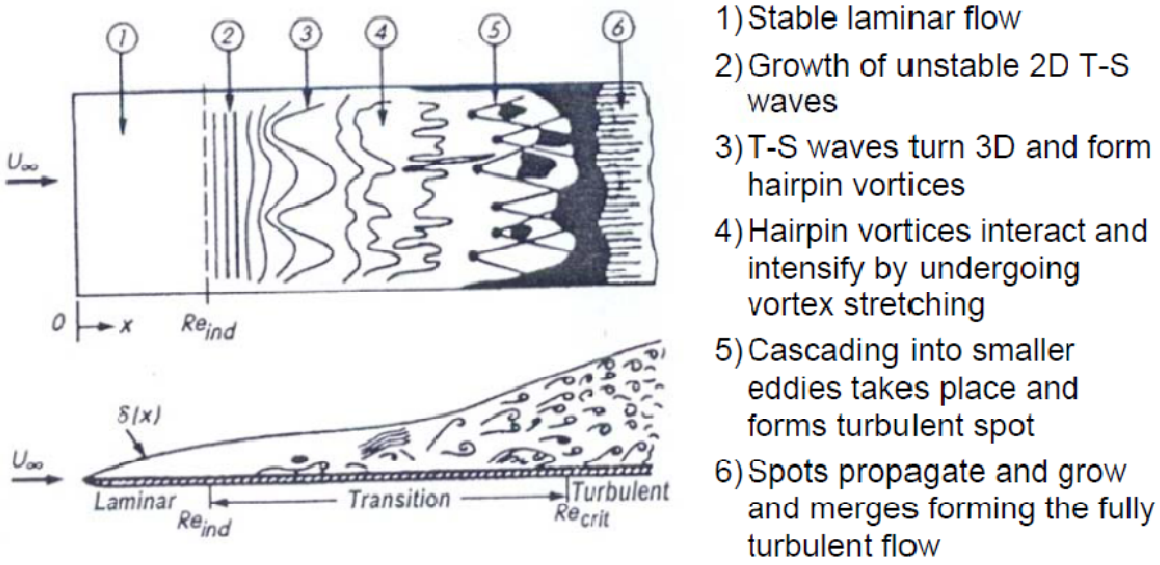

Figure 3.7 Laminar to turbulent transition process in a boundary layer [9]

3.6 Laminar separation bubble (LSB)

The performance of a model aircraft at low Reynolds numbers is strongly influenced by laminar separation bubbles. Such a separation bubble is caused by a strong adverse pressure gradient, which causes the laminar boundary layer to separate from the curved aerofoil surface. The separated laminar flow is highly sensitive to disturbances, which finally cause it to change to the turbulent flow. The transition region (not exactly a transition point) is located away from the aerofoil at the outer boundary of the separated flow area. The thickness of the turbulent boundary layer grows rapidly, forming a turbulent wedge, which may reach the aerofoil surface again. The region where the turbulent flow touches the surface again is called the reattachment point. The volume enclosed by the regions of separated laminar flow and turbulent flow is called a laminar separation bubble. Inside the bubble the flow may be circulating, the direction near the aerofoil surface may even be the opposite of the direction of the outer flow. There is almost no energy exchange with the outer flow, which makes the laminar separation bubble quite stable. The separation bubble thickens the boundary layer and thus increases the drag of

the aerofoil. The drag increment can be several times the drag of the aerofoil without a separation bubble. Lift and Moment are also influenced by a laminar separation bubble, which can lead to problems with stability and control of a model aircraft.

Figure 3.8 shows a schematic of an LSB. The boundary layer typically starts with a laminar boundary layer, but after encountering an adverse pressure gradient, this causes the boundary layer to separate. The laminar separated shear flow is unstable and transfers to a turbulent separated shear flow. The turbulent then transports momentum from the free-stream, across the shear layer, and down towards the surface. When the momentum transport is sufficient, the turbulent boundary layer reattaches to the surface, thus closing the separation bubble.

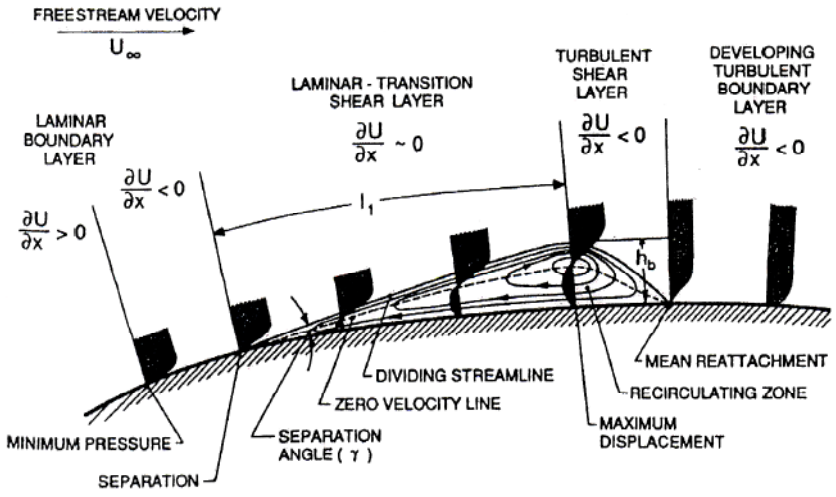

Figure 3.8 Description of a laminar separation bubble [91]

3.7 Boundary layer thickness determination

Boundary layer thickness is defined as the distance which is affected by viscous effect around a body immersed in fluid flow from the surface until the position normal to the surface reaches streamwise velocity about 99% of the freestream velocity.

The laminar boundary layer thickness can be calculated from the equation (2).

$$\frac{\delta}{x} = \frac{5.0}{Re_x^{1/2}} \qquad (2)$$

The turbulent boundary layer thickness can be calculated from the equation (3).

$$\frac{\delta}{x} = \frac{0.37}{Re_x^{1/5}} \qquad (3)$$

4. CFD simulations

In this project, a study of the aerodynamic characteristics was carried out by numerical simulation using the SA, kω-SST, and Transition-SST turbulence models. Lift and drag coefficients for a NACA 0015 aerofoil at different angles of attack for a velocity of 10m/s and Reynolds number of 650,000 were evaluated. For the analysis of turbulent flow generated around the aerofoil, the grid spatial resolution near the wall, y_+, must be small enough to capture the flow characteristics. A numerical simulation was made by Lee et al [92] to understand the effect of the angle of attack on a NACA 0015 aerofoil for making the vertical axis Darius wind turbine. The near-wall y+ value which is less than 1 is known to be most desirable for a near-wall modeling [92]. They investigate the optimum value of y+. The Reynolds number was 360,000, where the chord length and the velocity were 0.12m and 43.8m/s, respectively. They concluded that it is reliable and appropriate to use y+ value close to 1.

The investigation of the drag force and lift force acting on the airfoil was performed by a two-dimensional flow analysis. ANSYS-FLUENT was used for the interpretation of favorable flow characteristics near the wall with different turbulence models. The grid generator, ICEM CFD, was also used to create the meshes around the aerofoil and the flow domain. For this research, structured grid with quadrilateral elements was used in order to generate the domain around the aerofoil. To understand the phenomenon over the surface of the aerofoil the mesh density was high enough to evaluate the vortex, boundary layer and separation. The y+ and the number of grid points close to the surface dominate the variation of grid structure.

Turbulent flow was assumed for the entire flow field in order to derive the appropriate results in the Reynolds number of 650,000, where the entrance wind speed was 10 m/s. By varying the angle of attack 0° to 24° with an interval of 2°, except for the angles close to stalling which vary with interval of 1°, the lift coefficient and drag coefficient effects were analyzed for the NACA0015 aerofoil.

4.1 Grid independence study

Grid generation is a very important process in numerical simulation for CFD. The solutions of the simulations generally depend on constructions and numbers of the mesh. The solutions will be more accurate if the numbers of the mesh increase; however, this could be time consuming and impact on memory constraints. At first a coarse mesh should be generated to be used

for a simulation and then a finer mesh will be adopted to get closer the accurate solution. The repeat procedure with finer mesh simulations is carried out. If the coarse mesh gives a solution which is invariant with the finer meshes, Grid independence is achieved and the coarse mesh is used for further analysis.

Grid independence study was carried out in this project. C-type mesh, which is a very good mesh for aerofoil simulation because it can better fit than other meshes to the aerofoil surface, was selected and constructed around an NACA 0015 aerofoil. The numbers of node 200, 400, 600, and 800 were constructed to conduct Grid Independence Study at 6° of angle of attack at a Reynolds number of 650,000 (V= 10m/s, aerofoil chord = 1m). Turbulence models which were applied to the simulations are kω-SST, transition-SST, and SA models. Mesh with 400 nodes around the aerofoil was constructed as Figure 4.1a, b.

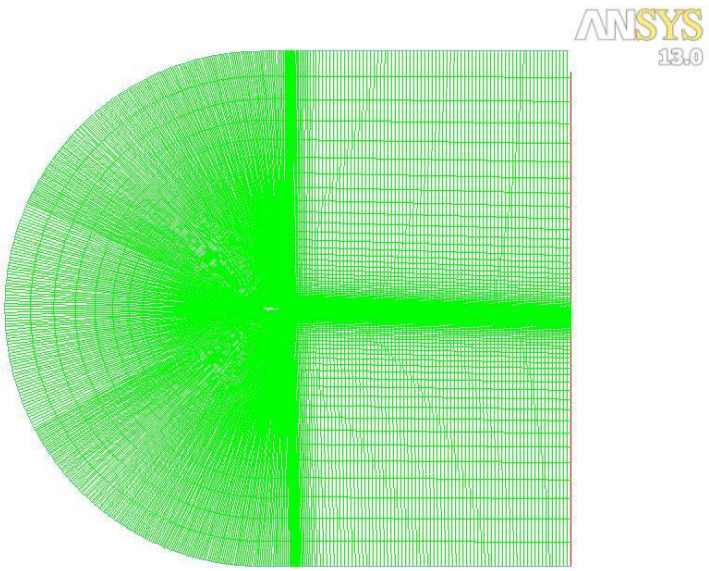

(a)

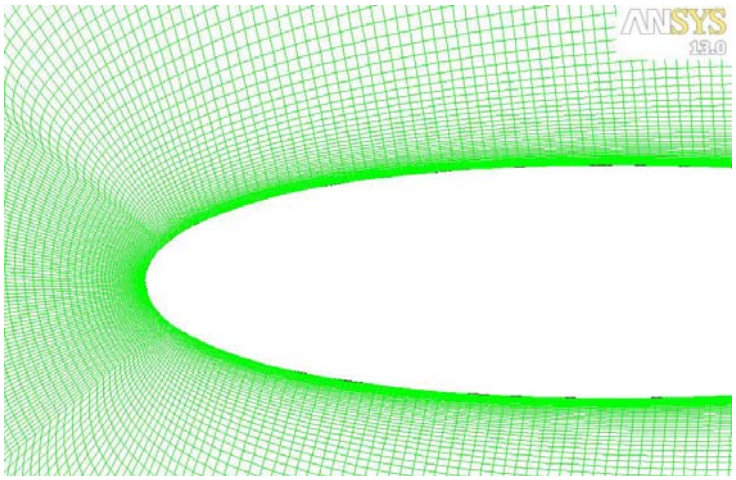

(b)

Figure 4.1 Mesh construction with 400 nodes around the leading edge of a NACA0015 aerofoil

Figure 4.2 shows that the number of the mesh with 400 nodes around the aerofoil is sufficient to simulate the flow for this aerofoil because C_l does not change with the increased nodes. Transition-SST model gives the best solution when compared with kω-SST and SA models because the line is closer to the experimental data line.

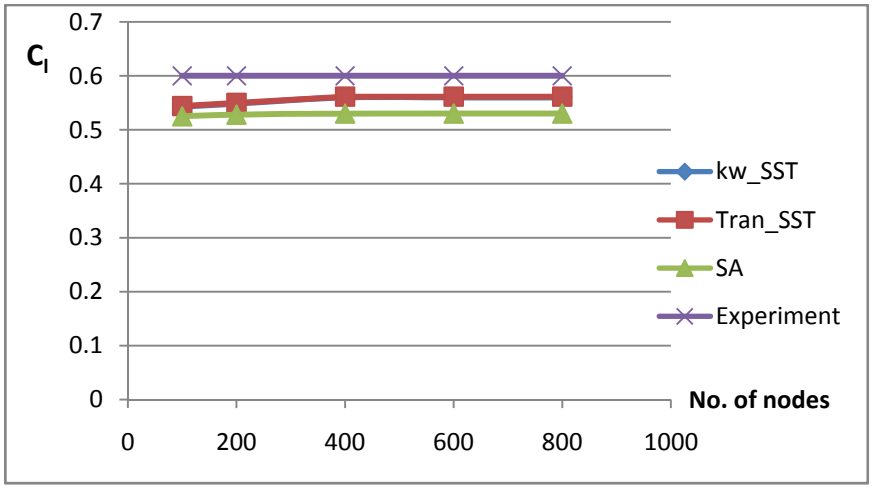

Figure4.2 Grid independence study, C_l vs. Numbers of nodes

Figure 4.3 shows that the number of the mesh with 400 nodes around the aerofoil is enough because C_d does not change with the increased nodes.

Transition-SST model gives the best solution when compared with kω-SST and SA models because the line is closer to the experimental data line.

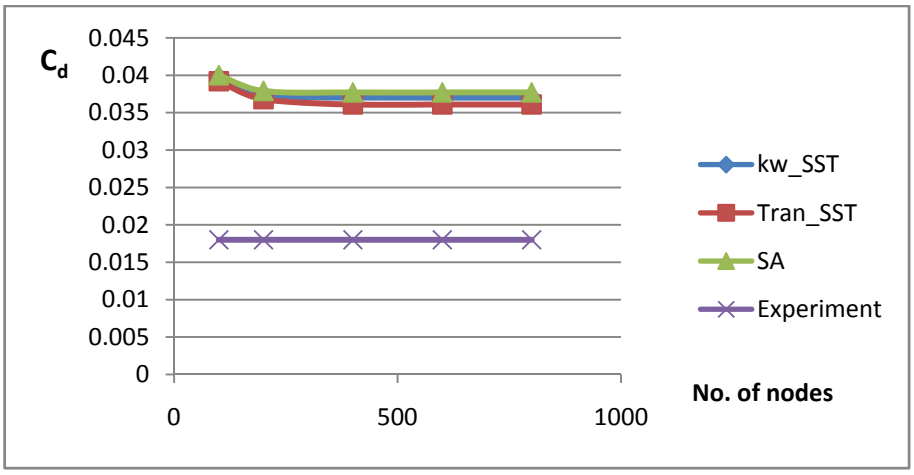

Figure 4.3 Grid independence study, Cd vs. Numbers of nodes

As a result of the Grid Independence Study, the number of 400-nodes mesh was chosen for further analysis.

For CFD simulation the placement of the first node in near-wall inflation mesh is very important. The y+ value is a non-dimensional distance from the wall to the first mesh node. To use a wall function approach correctly, y+ must be within a certain range. The first node of the grid line normal to the surface must fall inside the boundary layer region. If this does not happen, then the Wall Functions used by our turbulence model may incorrectly calculate the flow properties at this first calculation point which will introduce errors into our pressure drop and velocity results. To determine the distance between the first node and the wall(y), wall distance, the y^+ must be specified. The equations used to calculate the wall distance(y) are shown below:

$$y = \frac{y^+ \mu}{\rho u_*}$$

$$u_* = \sqrt{\frac{\tau_w}{\rho}}$$

$$\tau_w = C_f . \frac{1}{2} \rho U_\infty^2$$

$$Re_x = \frac{\rho U_\infty x}{\mu}$$

$$C_f = [2logRe_x - 0.65]^{-2.3} \; for \; Re_x < 10^9$$

(from Schlichting skin-friction correlation)

For example, if Re_x = 660,000, air velocity = 10 m/s, air density = 1.205 kg/m^3, dynamic viscosity of air = 1.82x10^{-5} kg/m.s, x = 1 m and y^+= 1, the wall distance will be about 3.38x10^{-5} m. That means that the first node is at a point far from the wall 3.38x10^{-5} m.

Alternatively, the calculation of y is simple by using "Y+ Wall Distance Estimation" tool from CFD Online website [93] as shown in Figure 4.4.

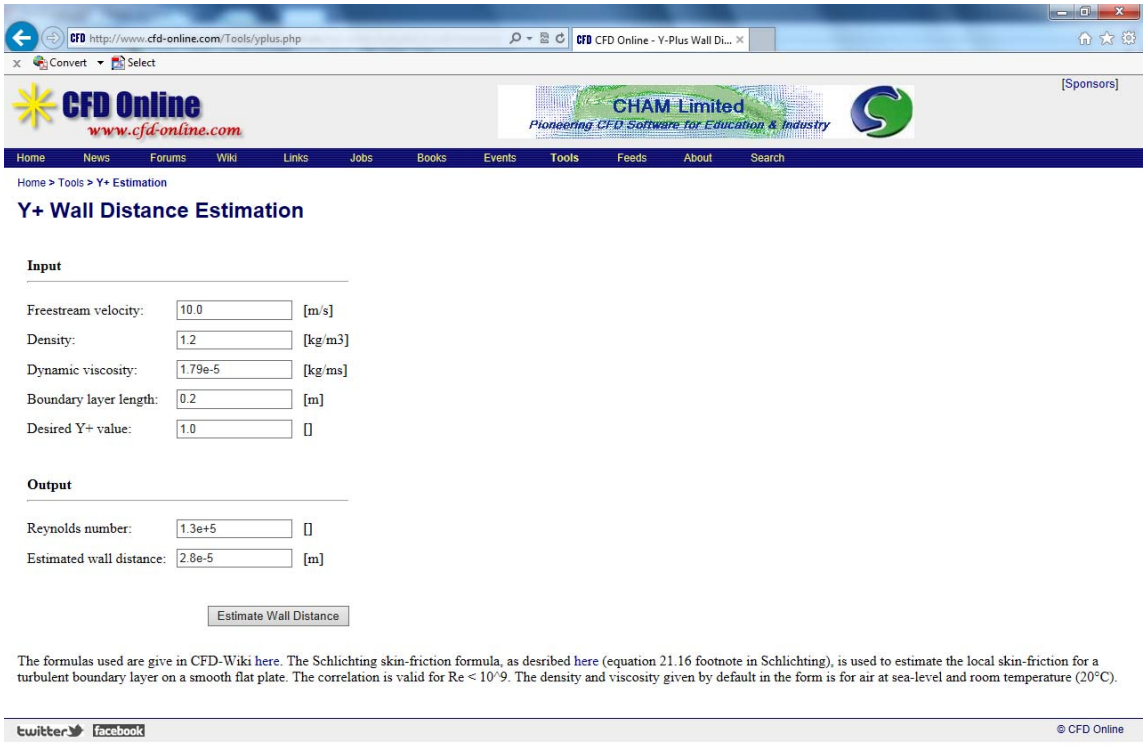

Figure 4.4 y+ wall distance estimation from CFD Online website [93]

The wall y+ values of the simulation of the flow around the NACA0015 aerofoil are exhibited in Figure 4.5.

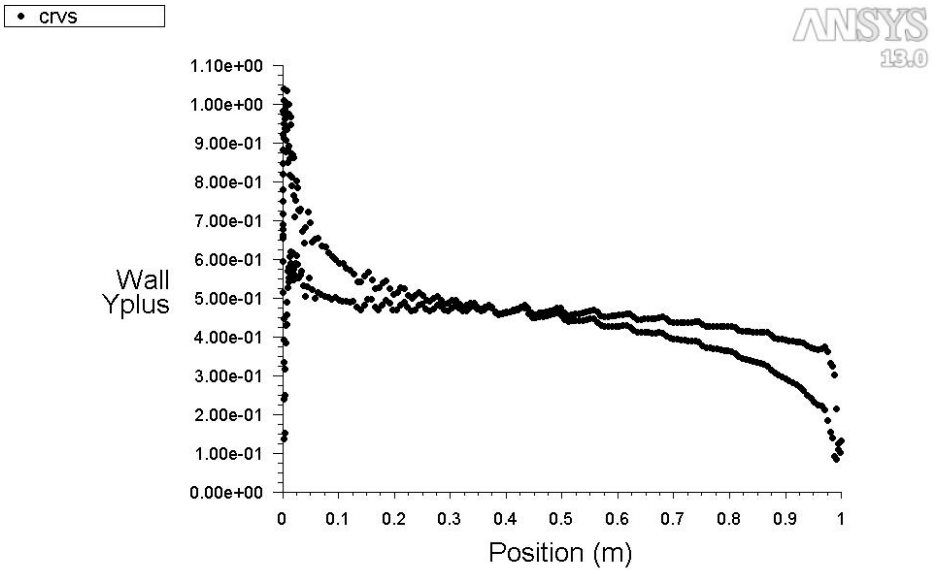

Figure 4.5 Wall y+ over the aerofoil on both sides

4.2 Results and discussion

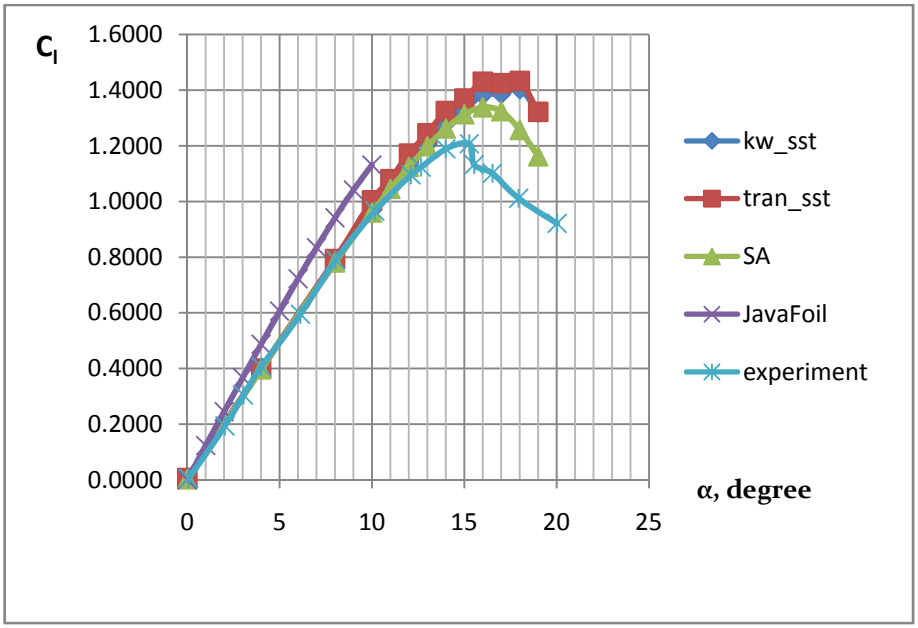

Figure 4.6 C_l vs. α of each Turbulence model and experimental results

At the flow condition having Re = 650,000 (V=10m/s, c=1m), Cl VS α were plotted with various turbulence models in Figure 4.6. These turbulence models show the outcome in good agreement with the experimental result from 0° to 9° of angle of attack. At an angle of attack greater than about 10° the result starts to have little difference from the experiment. The obvious

difference can be seen after 12°. Stall angle of the turbulence models are higher than that of the experiment. This is possibly due to the mesh construction. From the Figure 4.6 the kω-SST and Transition-SST turbulence models give similar results because they hold similar equations to solve the flow, while SA model has only one equation but can solve the flow better. The results show that these turbulence models cannot capture the flow well as good as expected when the angle of attack is greater than 12°, where the strong adverse pressure gradient significantly affects the flow and makes it to separate from the aerofoil surface. It is recommended that other simulations, which are more effective, such as, LES, DES, and DNS, should be applied to simulate the flow for better results, but these consume more memory and time expense.

Figure 4.7 shows the relation between Cl and Cd (drag polar) with different turbulence models. The turbulence models give higher drag coefficient than that from the experiment. The Cd is considerably different from the experimental results. This implies that the mesh construction was not built precisely for capturing the flow characteristics. In addition, the trailing edge of the aerofoil in CFD simulation is sharper than that of the aerofoil from the experiment so this would result in different pressure distribution as well as a separated flow region on the aerofoil. These causes can produce higher lift and higher drag than usual. It is recommended that other simulations, which are more effective, such as, LES, DES, and DNS, should be applied to simulate the flow for better results, but these consume more memory and time expense.

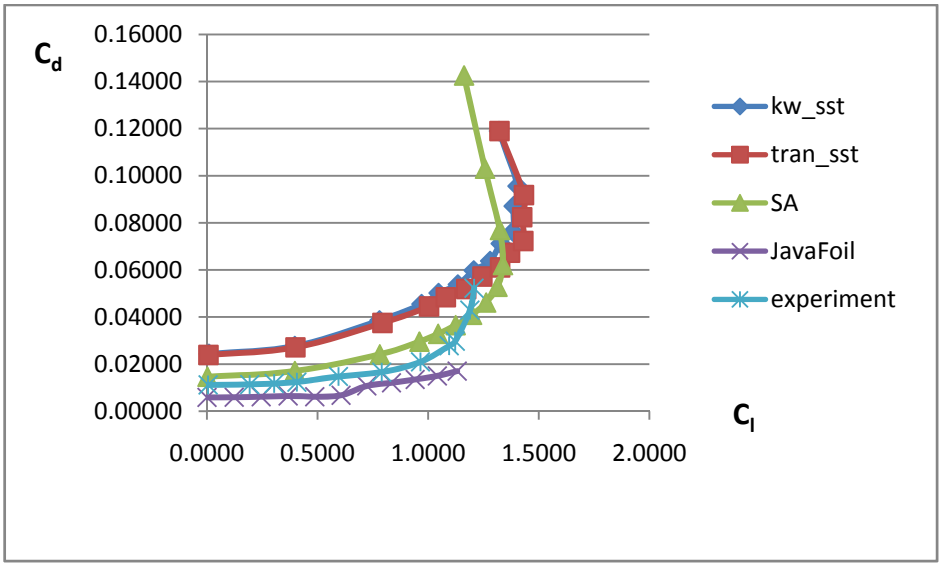

Figure 4.7 C_d vs. C_l of each Turbulence model and experimental results

An example is given for the flow around the aerofoil at an angle of attack of 4°. Figure 4.8 shows the velocity vector occurring around the aerofoil. Free stream velocity of 10 m/s is decelerated to 0 m/s near the leading edge and then is accelerated at the upper surface nearby the leading edge to maximum velocity about 14.5 m/s and again the velocity is decreased to 0 m/s nearby the trailing edge. On the other hand (Figure 4.9) the pressure around the aerofoil drops as the wind velocity increases and vice versa.

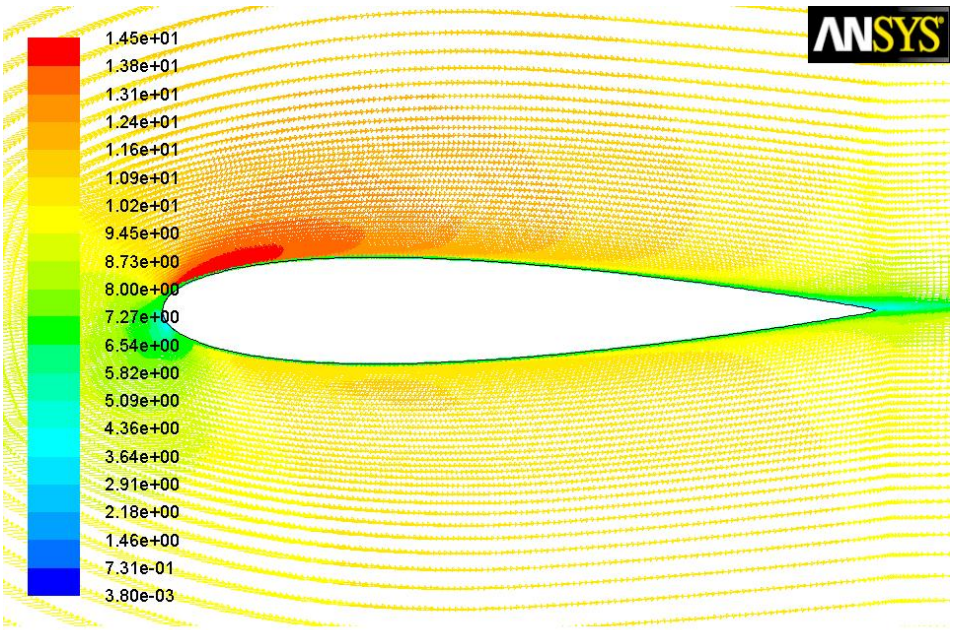

Figure 4.8 Velocity vector around NACA0015 at 4°

Figure 4.9 shows the pressure coefficient around the aerofoil at 4° of angle of attack. The lower line represents the pressure coefficient of the upper surface of the aerofoil (called suction side) whereas the upper line represents that of the lower surface of the aerofoil. This figure shows that the upper surface has lower static pressure than atmospheric pressure and sucks in the air flowing around the aerofoil. The lower surface has a larger pressure coefficient than that of the upper surface. As a result of the difference of pressure distribution between the upper surface and the lower surface, this generates lift which makes the wing float in the air.

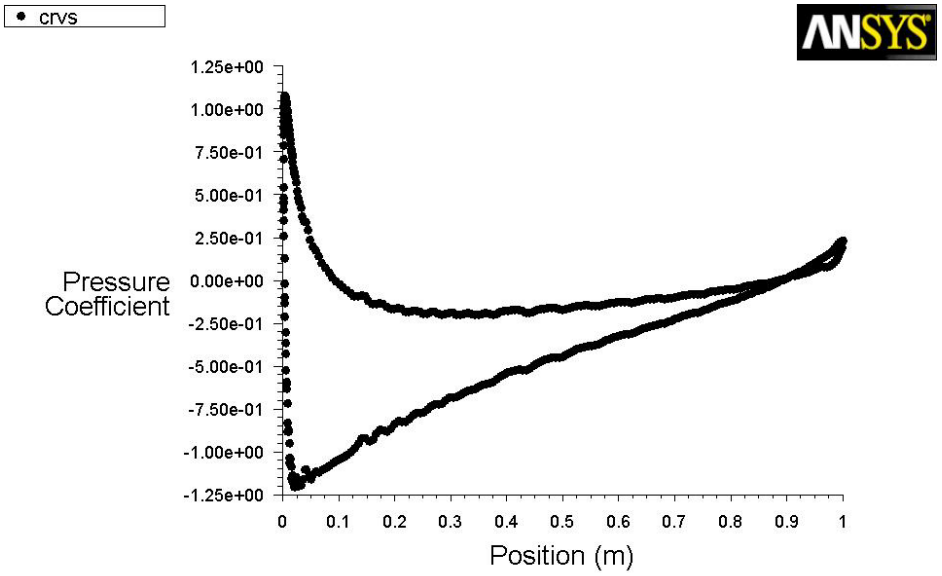

Figure 4.9 Pressure coefficients around the aerofoil at 4°

When an aerofoil has a sufficiently high angle of attack (depending on each type of aerofoil), flow separation and reversed flow can occur. For the simulation of NACA0015 aerofoil (Figure 4.10) the separation and reversed flow occur at about an angle of attack of 18° on the top of the trailing edge because of higher pressure and lower velocity.

Pressure gradient is one of the factors that influences a flow immensely. It is easy to see that the shear stress caused by viscosity has a retarding effect upon the flow. This effect can however be overcome if there is a negative pressure gradient offered to the flow. A negative pressure gradient is termed a favourable pressure gradient. Such a gradient enables the flow. A positive pressure gradient has the opposite effect and is termed the Adverse Pressure Gradient. Fluid might find it difficult to negotiate an adverse pressure gradient. When the air flows past the curved surface of the aerofoil, the favourable pressure gradient starts at the leading edge and up to a point before separation occurs. The negative pressure gradient will counteract the retarding effect of the shear stress (which is due to viscosity) in the boundary layer. Now the adverse pressure gradient begins to retard. This effect is felt more strongly in the regions close to the wall where the momentum is lower than in the regions near the free stream. As the velocity near the wall reduces and the boundary layer thickens, a continuous retardation of flow brings the wall shear stress at a point on the wall to zero. From this point onwards the shear stress becomes negative and the flow reverses and a region of recirculating flow develops. The flow no longer follows the contour of the body. This indicates that the flow has separated as

shown in Figure 4.10. The point where the shear stress is zero is called the Point of Separation.

Depending on the flow conditions, the recirculating flow terminates and the flow may become reattached to the body. A separation bubble is formed. There are a variety of factors that could influence this reattachment. The pressure gradient may be now favourable due to body geometry and other reasons. The other factor is that the flow initially laminar may undergo transition within the bubble and may become turbulent. A turbulent flow has more energy and momentum than a laminar flow. This can stop separation and the flow may reattach. A short bubble may not be of much consequence.

On the aerofoil, the separation occurs and gives rise to a short bubble. When the separation occurs more towards the trailing edge and the flow is not reattaching. In this situation the separated region merges with the wake and results in the stall of the aerofoil (loss of lift).

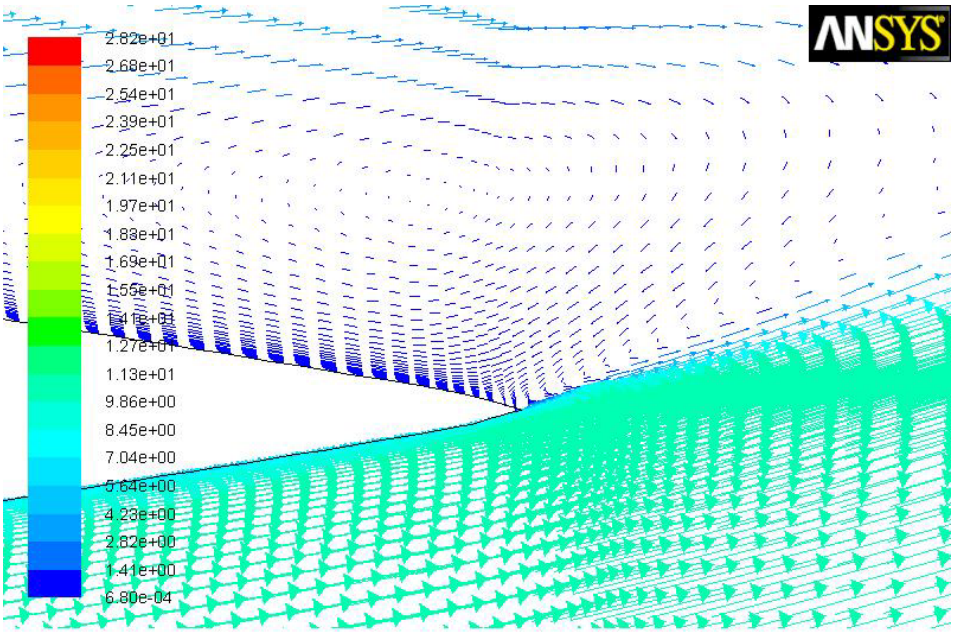

Figure 4.10 Trailing edge separation and reversed flow of the aerofoil at 18°

In the present study, a NACA0015 aerofoil model was selected in order to observe the aerodynamic characteristics against the angle of attack by using the SA, kω-SST, and Transition-SST turbulence models. The wall values y+ of 1 was taken as reference to investigate coefficients of lift and drag. The current results are summarized as follow;

1) The lift coefficients obtained were similar to the experimental results from NACA report No.586 in the range of the angles of attack between 0º and 10º. When the angle of attack is greater than 12º, the difference of lift coefficient appears to be obvious, especially at the angle above stall angle (15º). This may be because the construction of the mesh around the aerofoil was not generated appropriately to capture the flow in near-wall region and the flow characteristics, especially in separation flow.

2) Using numerical simulation of turbulent flows around the aerofoil, the turbulence models give higher drag coefficient than that from the experiment. The C_d is considerably different from the experimental results. This implies that the mesh construction was not built precisely for capturing the flow characteristics. In addition, the trailing edge of the aerofoil in CFD simulation is sharper than that of the aerofoil from the experiment so this would result in different pressure distribution as well as a separated flow region on the aerofoil. These causes can produce higher lift and higher drag than usual.

3) In this study, RANS was used to simulate the flow around the NACA0015 aerofoil. RANS has been used popularly in engineering applications because it requires less computational time and gives acceptable results for simulation close to the wall region. Nevertheless, it fails to predict the severely separated flows. LES approach provides more accurate turbulent structures for the separated flow by capturing the energy within the wake behind the separation flow, but this can consume large computational time, especially in the near-wall region. Hybrid RANS/LES approach is to model the small turbulence in the area close to the wall and resolve the larger turbulent structures elsewhere. DES approach is one of the most popular hybrid RANS/LES methods. It is recommended that DES or DNS should be used in order to better capture the separation flow characteristics.

5. Wing experiments

In the present study, the boundary layer trips (BLTs) were attached above the aerofoil surface at various sizes and locations to investigate the effect of the sizes and the locations on aerodynamic characteristics, especially lift and drag coefficient, at various angles of attack, both before and after stall at Reynolds number of 78,000. The lift and drag forces in case of normal NACA0015 aerofoil wing as well as the wing with boundary layer trips were measured by a six-component load cell, ATI NANO 43, and compared to each other and the experimental results from NACA report No.586 [105]. The scope of the experiment was focused on attaching only one boundary layer trip above the upper surface of the wing each time.

The wing was designed by SolidWorks program and produced by using a CNC machine to mill wood giving many pieces of aerofoil-shaped wood. Assembly was required to build up the wing from many pieces of wood. This process made it easier to build the large wing, but the smoothness of the surface need to be taken care of. The wing surface must be scrubbed with sandpaper to reduce the effect from skin friction drag. The complete wing have a 0.2 m chord and 0.7 m wing span, which was installed in the centre of the wind tunnel test section (1.2mx1.2m) to get the maximum wing span and to avoid boundary layer effect at the wind tunnel side wall.

5.1 Aerodynamic characteristics of a NACA 0015 aerofoil wing with and without boundary layer trips

5.1.1 Objective

The objective of the experiment was to investigate the effect of boundary layer trips on a NACA 0015 aerofoil's performance at a low Reynolds number of 78,000. The goal of the experiment is to measure C_l, and C_d in case of the wing without boundary layer trip and with boundary layer trip. To do this a wing model of NACA 0015 aerofoil section, with and without boundary layer trips, with a 0.2 m chord and 0.7 m wing span was installed with the force transducer in the 1.2mx1.2m low speed wind tunnel of the University of Sheffield. At a speed of 6 m/s, aerodynamic force values were taken at angles of attack between 0 and 22 degrees. Then C_l and C_d values were calculated based on those data.

5.1.2 Apparatus and instrumentation

The experiments were conducted in the Mechanical Engineering's subsonic wind tunnel located at The University of Sheffield. This is a low turbulence, open-loop atmospheric wind tunnel capable of tunnel velocities of 25m/s. NACA 0015 wing is made of wood. The wing was mounted in the center of the test section. The wing has a constant chord of 0.2 m and a wing span of 0.7 m. The angle of attack is measured by digital angle gauge and is adjusted manually.

The wing model was connected via a load cell, an amplifier and, a board to a data acquisition computer as shown below in Figures 5.1 and 5.2. A total pressure Pitot-static probe is mounted inside the test section connected to an instrument to read airspeed of the flow. The ATI NANO43 load cell is capable to measure small forces very sensitively with the resolutions of 1/128 N for measured forces and 1/10 Nmm for measured torques. However, this small load cell has a sensitive range for measuring forces no more than 36 N and 500Nmm for torques. As a result, it should be remembered when designing the wing and installing the wing with the load cell, and also the experiment needs to be conducted very carefully to not to break the load cell.

The boundary layer trips attached on the wing are carbon fiber tube with 600 mm long and diameters of 6, 4, 3, and 1.5 mm respectively.

Figure 5.1 Low speed wind tunnel and data acquisition computer

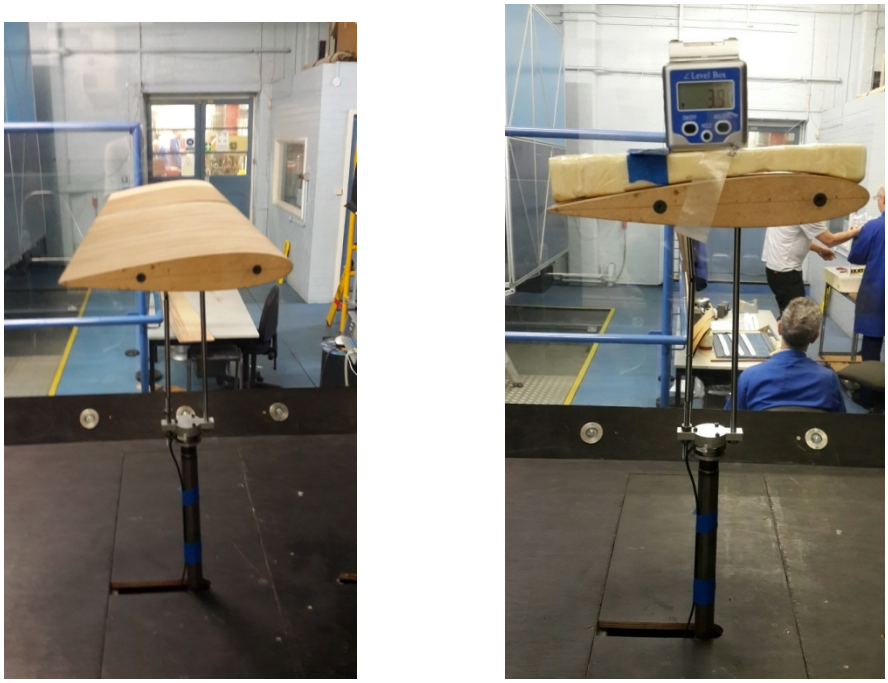

Figure 5.2 Installation of the NACA0015 aerofoil wing and angle of attack setting

5.1.3 Experimental procedure

The procedure for these experiments starts with installing the aircraft wing model of NACA 0015 and then levelling the wing for zero angle of attack. Then resetting the force and moment values on the screen in Figure 5.3 to zero. After this the wind tunnel is switched on to an airspeed of 6 m/s (Re = 78,000), waiting for a while for steady flow condition, and then the values on the screen are recorded for 10 times to make an average. The wind tunnel is then turned off and the process repeated with angles of attack of 2 to 22 degrees by 2 degrees increment each step. When the values of all angles of attack have been recorded, attach boundary layer trip (carbon fiber tube) diameter of 6mm at position of 10%c from the leading edge with tape and start the procedure as the wing from 0 to 22 degrees then change the position of the trip to 20%, 30%, 40% ,and 50%c respectively. Repeat the experiments by changing the trip to diameter of 4mm, 3mm, and 1.5 mm respectively. When all results are received, calculate C_l, and C_d as well as plot graphs C_l VS α and C_d VS α.

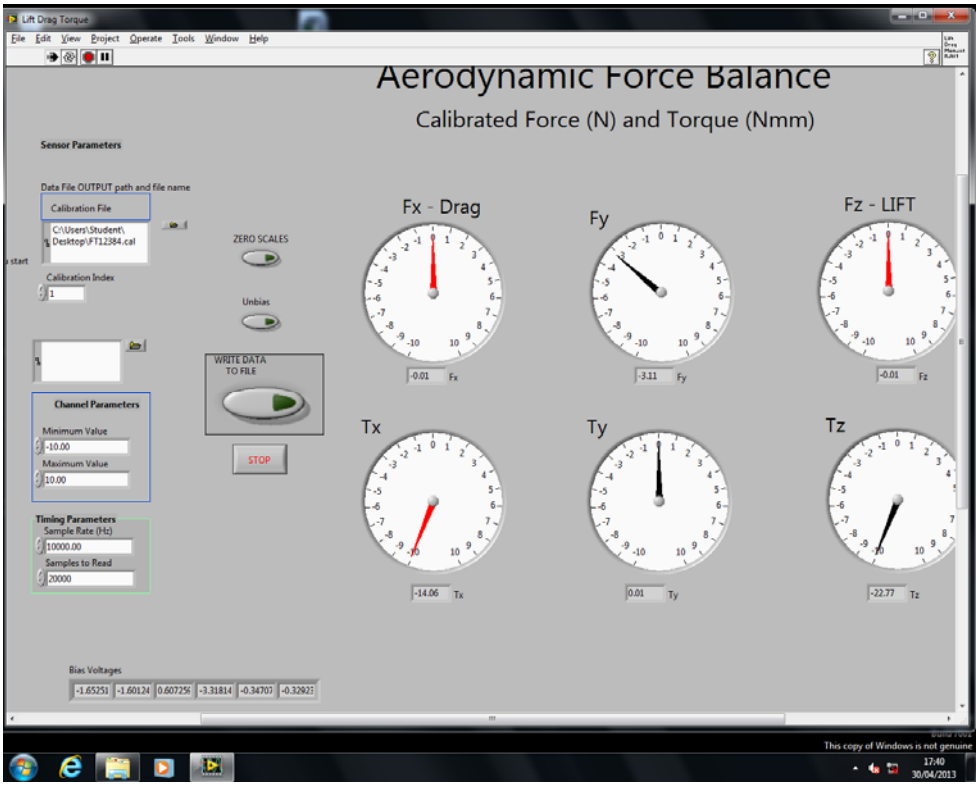

Figure 5.3: The program for recording aerodynamic forces and moments

5.1.4 Results and discussion

Results are illustrated in Figures 5.4 to 5.15. Figures 5.4 and 5.5 represent lift and drag coefficients of the wing without boundary layer trip. Three-dimensional aerofoil (Wing) tested is compared to two-dimensional aerofoil. When the wing was at low angles of attack, there was no boundary layer separation along the wing; therefore, the velocity defect area behind the wing was small. At an angle of attack of about 14 degrees, there was boundary layer separation which led to a stagnation area on the back half of the wing and a loss of lift. From the angle of attack of 18 degrees, there is leading edge separation and a stagnation area along the entire wing as well as a significant loss of lift. From the data gathered from the force transducer the lift and drag coefficients of the wing can be calculated. During 0-14 degrees angle of attack, the lift coefficient is linearly increased while the drag coefficient is increased dramatically as the angle of attack greater than 15 degrees. These differences indicate that from 15 degrees the wing is post stall while the wing between 0 and 14 degrees has not stalled.

At an angle of attack greater than 14 degrees, there was boundary layer separation, which resulted in the stalling of the aerofoil, making the lift

coefficient drop suddenly, whereas the drag coefficient rapidly increases due to a greater pressure drag from separated flow effect.

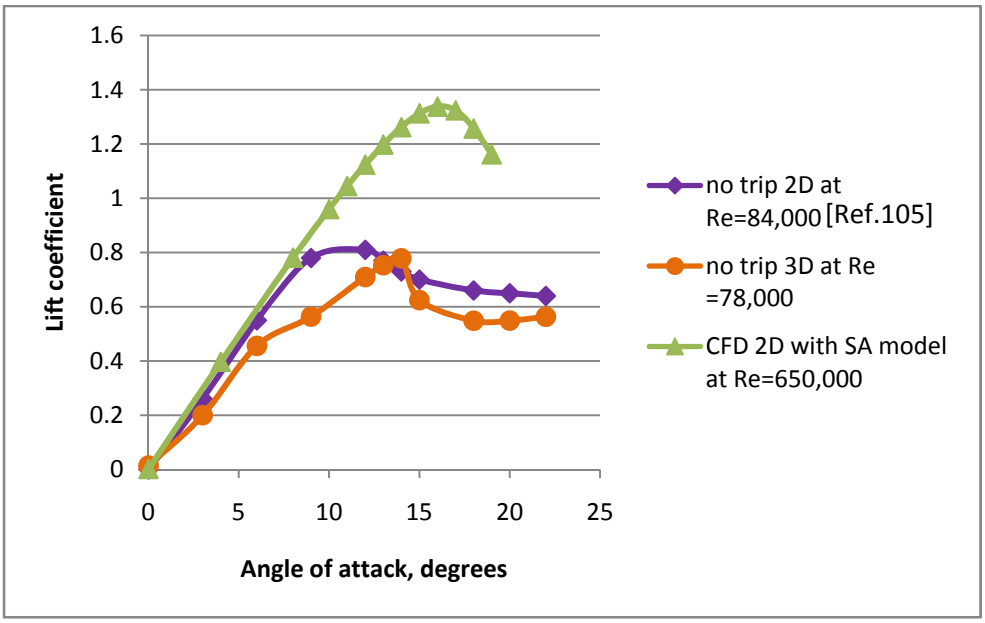

Figure 5.4 Comparison of lift coefficients of a NACA 0015 between experiments and CFD

From thin aerofoil theory, the slope of the C_l curve in linear region is equal to 2∏/radian (6.28/radian). This value is different from the slope of C_l from the experimental result of the NACA report No.586 [105] which shows that the slope of C_l for the two-dimensional straight wing is about 4.57. This is because thin aerofoil theory is good for approximation for the aerofoil which is quite thin but NACA 0015 aerofoil is a bit thick. From Figure 5.4, if we calculate the 3D lift curve slope, the slope will be 3.18 approximately. The 3D lift curve slope from Figure 5.4 differs from the 2D experimental result from NACA report No.586 [105] because it is a finite wing. The flow characteristics between 2D and 3D wing are definitely different because of downwash. This downwash results in a decrease in lift and an increase in drag, so it makes the lift slope is lower than that of 2D wing. A correction can be done by applying Helmbold's equation for low-aspect-ratio straight wing (incompressible).

$$a = \frac{a_0}{\sqrt{1 + (\frac{a_0}{\pi AR})^2} + \frac{a_0}{\pi AR}}$$

For NACA 0015 aerofoil, in the case of the 3D wing, the corrected lift curve slope from NACA report No.586 [105] will be about 3.05. It is found that this value is very close to the lift slope from the experiment in Figure 5.4 (lift curve slope = 3.18). This indicates that the experimental results are in good agreement with the theory.

When comparing the CFD results (SA model), having the flow condition of Re = 650,000 (V=10m/s, c=1m), with the experimental results (Re = 78,000), the difference can be seen due to the difference in Reynolds number as well as flow dimension. The result from CFD is a two-dimensional flow while the results from the experiments have both two-dimensional flow (NACA report No.586 [105]) and three-dimensional flow, conducted in this project.

For drag coefficient the experimental results (3D wing) in Figure 5.5 show that the drag coefficients are higher than that of two-dimensional aerofoil because of induced drag introduced by wing-tip vortices. However, the NACA0015 aerofoil wing was not well constructed enough. It was deliberately left rough and the plan was to smooth it out for the next step, so this will cause higher skin friction drag than usual wing. In addition, the wing was connected to struts when conducting the experiments. This is obvious that not only parasite drag and induced drag from the wing occur but also parasite drag of struts and interference drag between the wing and the struts occur. Thus, total drag for 3D wing tested consists of parasite drag, induced drag due to the wing and struts, as well as interference drag from connecting the wing with the struts.

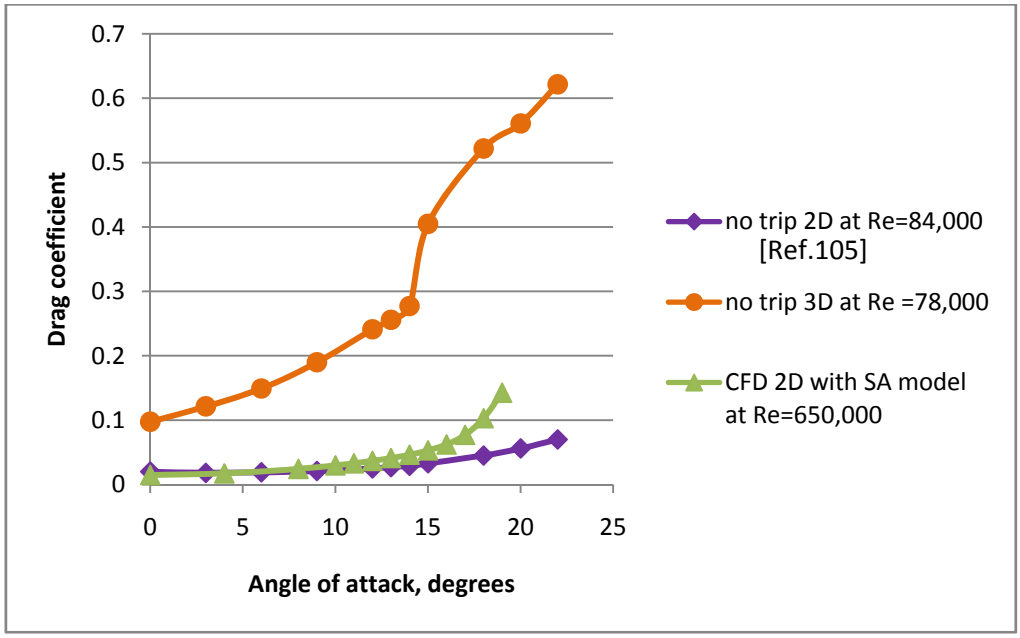

Figure 5.5 Comparison of drag coefficients of NACA 0015 between experiments and CFD

Figures 5.6, 5.8, and 5.10 have very similar trends for the C_L curve. These figures show lift coefficients of BLT height of 6, 4, and 3 mm located at 10%, 20%, 30%, 40%, and 50%c from the leading edge and compared to the wing without BLT. The results indicate that 6, 4, and 3 mm height BLT for all positions gives lower C_L compared to the normal wing almost angles of attack, except for the angles from 18° to 22°. When the angles are larger than 18°, BLTs can alleviate the stall and increase C_L. This may be because the size of LSB was reduced and the separation flow reattached downwards to the wing surface due to energized separated boundary layer. It is observed that for each BLT height, the location that generated highest C_L is at 50%c. In addition, a benefit of BLT is that it makes the stall less severe than the normal wing because reattachment of the separated boundary layer. This could be confirmed by C_L graphs of the wing with BLT. Nevertheless, BLT should be located at the distance from 20%c downwards the leading edge. The optimum location should be at 50%c because this results in maximum lift coefficient and minimum drag coefficient.

Figures 5.7, 5.9, and 5.11 tend to have similar C_D characteristics. These figures show drag coefficients of BLT height of 6, 4, and 3 mm located at 10%, 20%, 30%, 40%, and 50%c from the leading edge respectively and compared to the wing without BLT. The results indicate that 6, 4, and 3 mm height BLT for all positions gives more C_D compared to the normal wing almost angles of attack, except for the 4mm height BLT located at 50%c. Flow visualization and pressure distribution survey is needed to make this clear. When the angles of attack larger than 18°, BLTs can alleviate the stall and decrease C_D. This may be because the size of LSB was reduced and the separation flow reattached downwards to the wing surface. It is observed that for each BLT height, the location where generated lowest C_D is at 50%c.

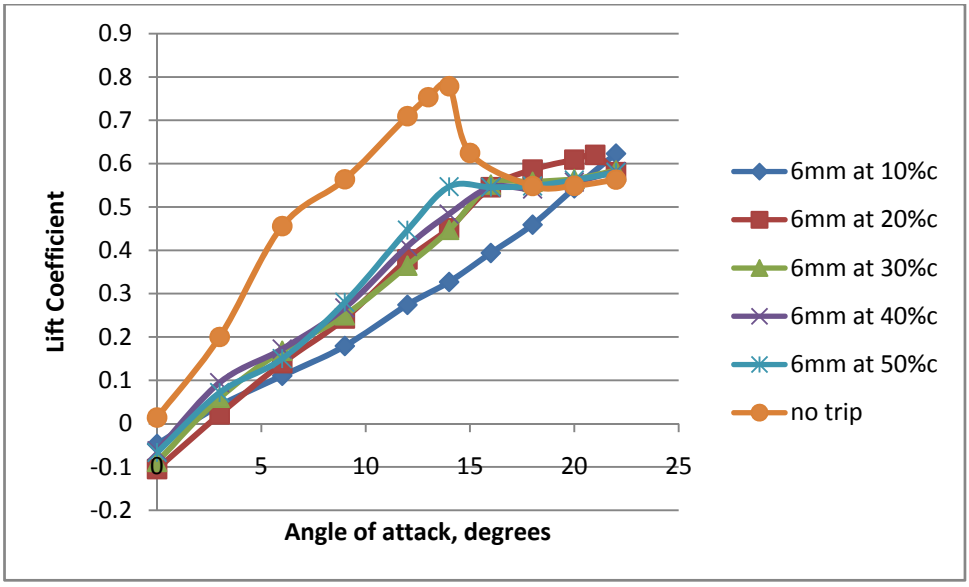

Figure 5.6 C_L vs. α of boundary layer trip 6mm diameter at Re = 78,000

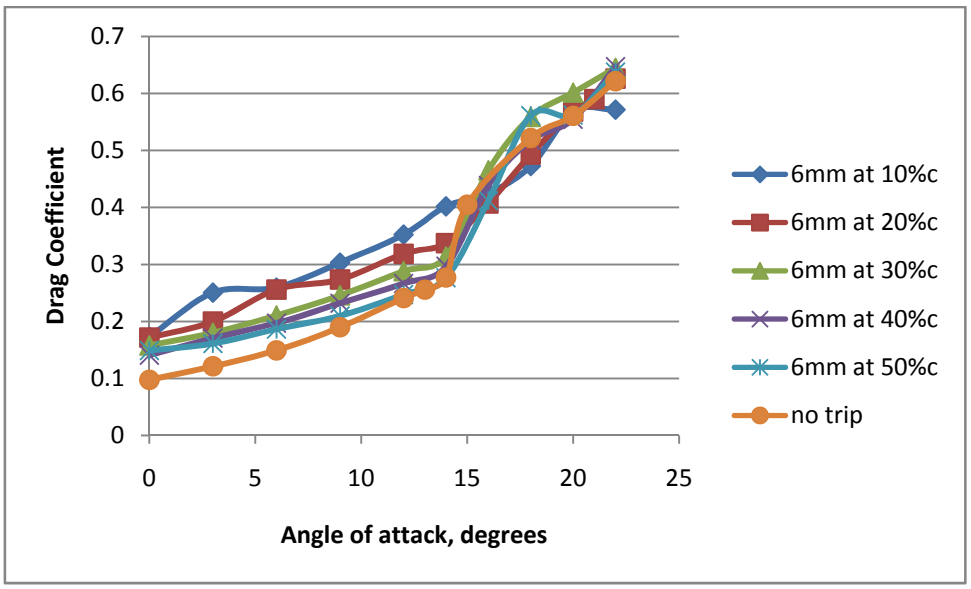

Figure 5.7 C_D vs. α of boundary layer trip 6mm diameter at Re = 78,000

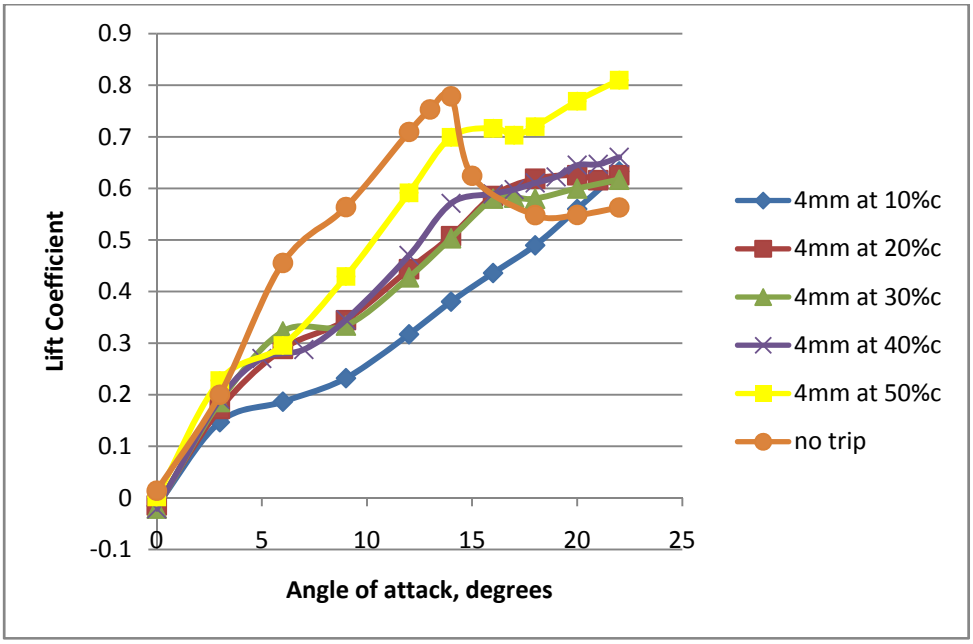

Figure 5.8 C_L vs. α of boundary layer trip 4mm diameter at Re = 78,000

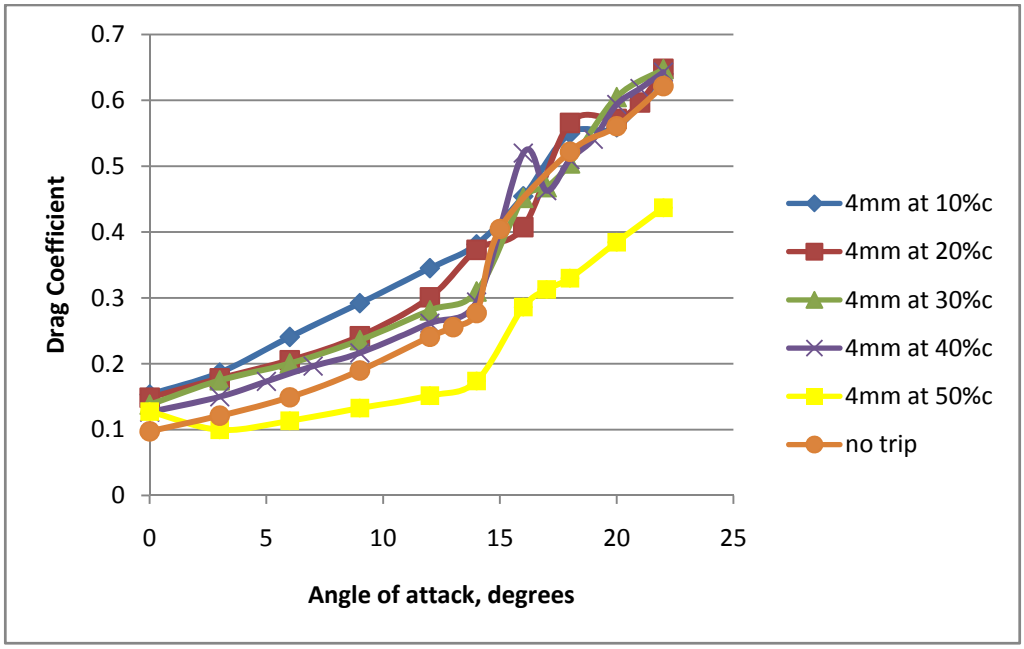

Figure 5.9 C_D vs. α of boundary layer trip 4mm diameter at Re = 78,000

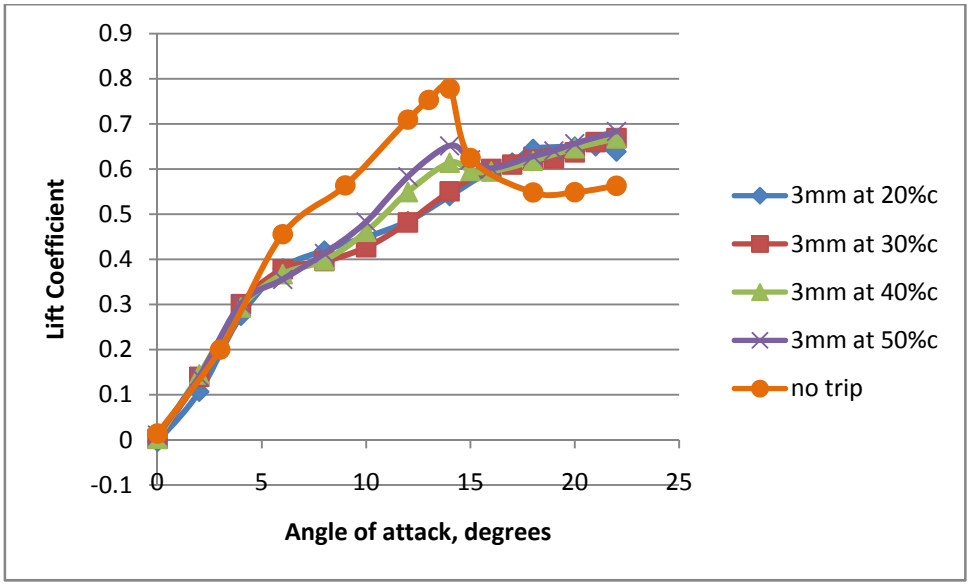

Figure 5.10 C_L vs. α of boundary layer trip 3mm diameter at Re = 78,000

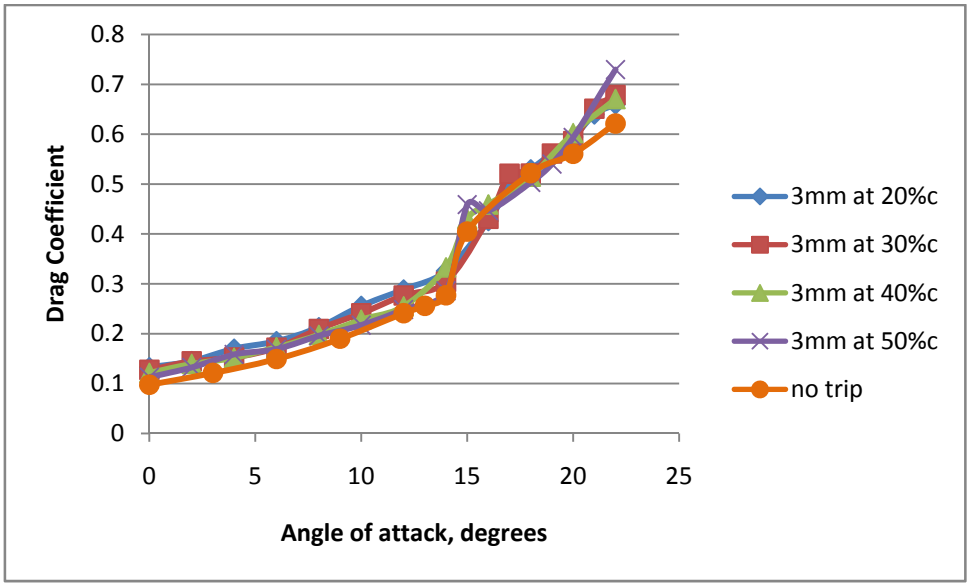

Figure 5.11 C_D vs. α of boundary layer trip 3mm diameter at Re = 78,000

Figure 5.12 shows the lift coefficients of BLT height of 1.5 mm located at 30% and 50%c from the leading edge and compared to the wing without BLT. The results indicate that the BLT for both positions gives C_L very close to the normal wing between the angles of attack 0° and 12°. When the angles are larger than 16°, BLTs can alleviate the stall and increase C_L above the normal wing. This may be because the size of LSB was reduced and the separation

flow reattached downwards to the wing surface due to energized separated boundary layer. It is observed that for each BLT height, the location that generated the highest C_L is at 50%c but the BLT located at 30%c has a bit higher stall angle. Unlike the former BLTs, the BLT height of 1.5mm did not make the stall less severe than the normal wing because of the reduced efficiency in reattachment of the separated boundary layer. This can be confirmed by C_L graphs of the wing with BLT. The optimum location should be at 50%c because this results in maximum lift coefficient and minimum drag coefficient.

Figure 5.13 shows drag coefficients of BLT height of 1.5mm located at 30% and 50%c from the leading edge respectively and compared to the wing without BLT. The results indicate that 1.5 mm height BLT gives C_D very close to the normal wing.

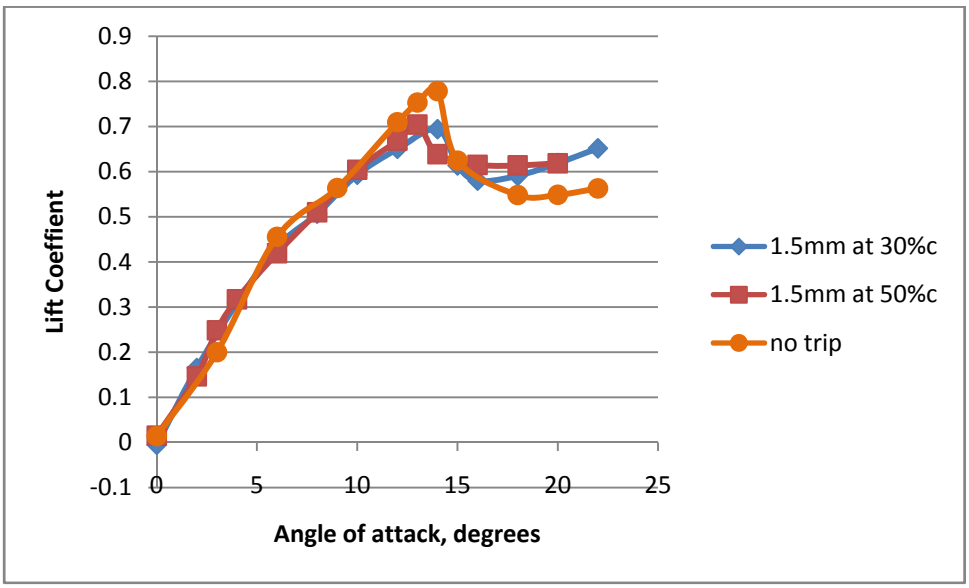

Figure 5.12 C_L vs. α of boundary layer trip 1.5mm diameter at Re = 78,000

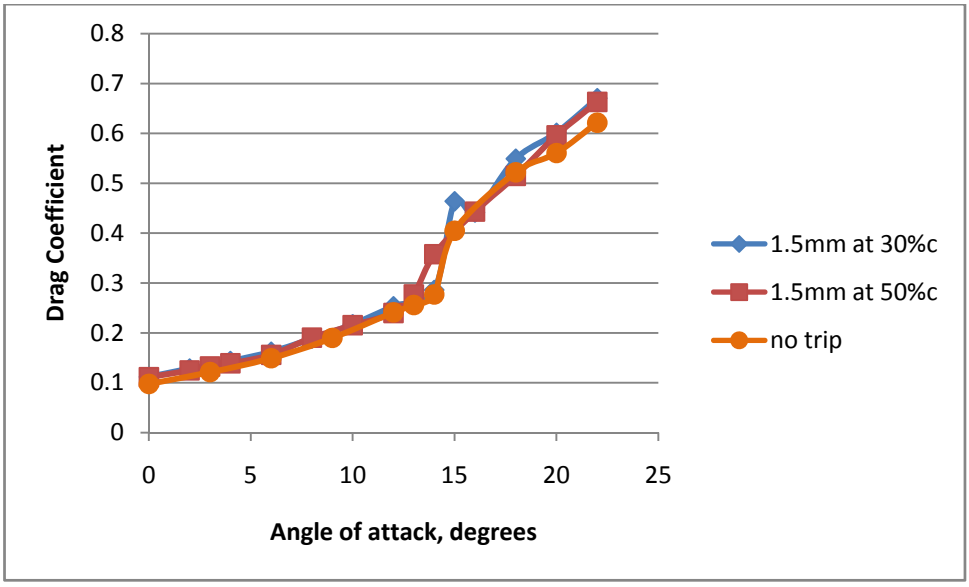

Figure 5.13 C_D vs. α of boundary layer trip 1.5mm diameter at Re = 78,000

Figure 5.14 shows lift coefficients of BLT height of 6, 4, 3, and 1.5 mm located at 50%c from the leading edge and compared to the wing without BLT. The results state that 6 mm height BLT located at 50%c produced lowest C_L while normal wing without BLT produced highest C_L for angles of attack between 0° and 14°. However, if the BLT height is lower than 6 mm, this makes the buffet manner, which is oscillations of an wing's structure caused by separated flow or turbulent airflow, after stalling less severe because the laminar separation bubble transform to turbulent boundary layer and reattach to the wing surface making smaller the region of the LSB. This also results in the generation of more lift as the angle of attack is increased greater than 15°. This can be confirmed by C_L graphs of the wing with BLT. An advantage of the wing with the boundary layer trips on lift coefficient can be seen on the graphs after stalled angle. The lift coefficient gradually decreases after stalling resulting in better stalling characteristics compared with no trip wing.

Figure 5.15 shows drag coefficients of BLT height of 6, 4, 3, and 1.5 mm located at 50%c from the leading edge respectively and compared to the wing without BLT. The results indicate that 4 mm height BLT generated lowest C_D compared to all cases both the normal wing and the wing with BLT.

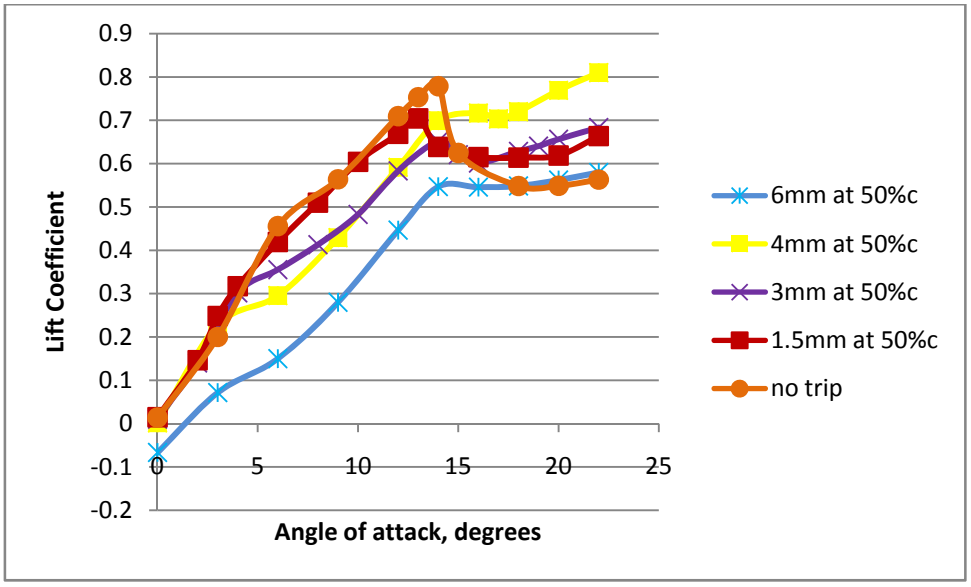

Figure 5.14 C_L vs. α of various boundary layer trips at Re = 78,000

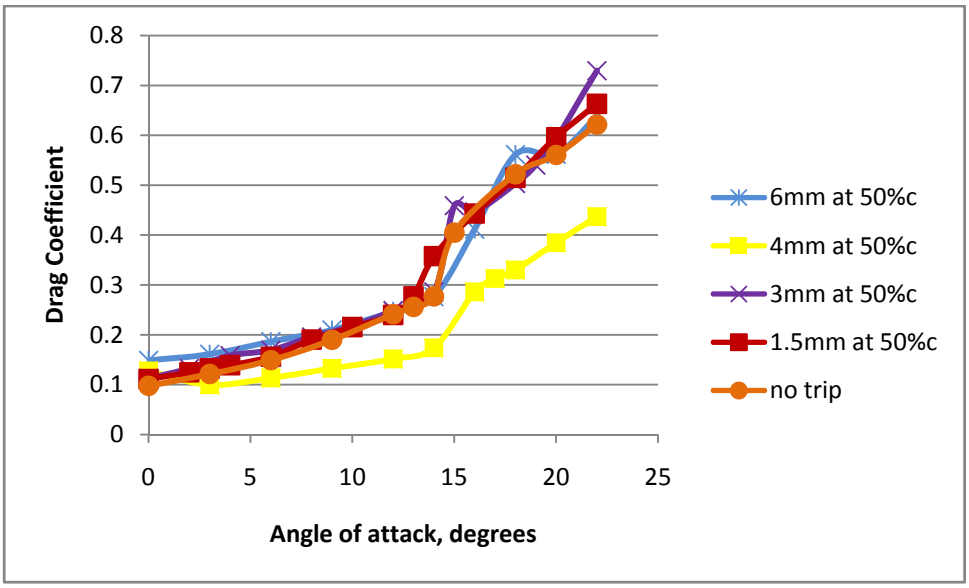

Figure 5.15 C_D vs. α of various boundary layer trips at Re = 78,000

The effects of the addition of a boundary layer trip to aerofoil's surface are variable depending on location and height (size). In general, it can be stated that the boundary layer trip located on the upper aerofoil's surface at 50%c has the most benefit in both lift coefficient increment and drag coefficient decrement when compared to the BLT located at other locations. However, the maximum lift coefficient at stall angle occurs in the case of no boundary layer trip. This implies that the pressure difference between the upper surface and the lower surface of the BLT case is lower than that of no BLT case. An advantage of BLT is that it makes the lift coefficient after stalling to

reduce more smoothly. When an angle of attack is greater than 15°, the lift coefficients in case of the BLT height of 1.5, 3, and 4 mm are higher than that of the wing with no BLT. This shows that it gives good effect when stalling occurs. For drag coefficient, only 4mm height of BLT can produce the less drag coefficient than the wing with no BLT. This is because the size of LSB is reduced. When using BLT, transition can be induced to occur at positions further forward the leading edge than not using the BLT. As a result, the flow changes from laminar to turbulent and this prevents the separated free shear layer and LSB to occur. When the flow entrains sufficient energy from the freestream, the separated free shear layer will reattach the aerofoil's surface. The experimental results are consistent with the experimental results by Huber II and Mueller [85] who indicated that trip wires located on the upper surface aft of the leading edge can significantly reduce maximum lift coefficient while improving or degrading minimum drag coefficient depending on the roughness height. Nevertheless, Huber II and Mueller [85] did not locate the trip wires at 10%c, 20%c, 40%c, and 50%c on the aerofoil's upper surface as this study and they used different aerofoils from this study.

Unfortunately, there is no literature that can exactly be compared the results with, since the authors used different aerofoil models, different BLT sizes, and locations. Lyon et al [79] tested several aerofoils with a variety of trip configurations and concluded that relatively thin trips were capable of producing fairly dramatic changes in drag for aerofoils with large bubbles. As trip heights increased, drag reduction was almost constant due to trade-offs made between device drag, skin friction drag, and bubble drag. The results from Lyon et al [79] slightly contrast to the results from this project. Lyon et al [79] indicated that as a trip was placed far upstream relative to the bubble, there was no advantage over one placed relatively close; thus, the trip can be placed as far forward as possible to prevent the trip to submerge within the bubble at angles of attack. On the other hand, in this project, the locations of the same trip fairly affect the flow characteristics and so give different lift and drag for different locations, except for 1.5 and 3 mm height trip that have similar results.

6. Conclusions and Recommendations

6.1 Conclusions

From the measured lift coefficient of the NACA0015 wing (no boundary layer trips), it is apparent that the aerofoil suffered a severe loss of lift somewhere beyond angles of 14 degrees. This is the point at which the flow separated from the suction side of the aerofoil causing the stalled condition. When applying Hembold's equation to the 2D experimental results from NACA report No.586 [105], the lift curve slope for a finite wing (3D) was obtained and compared to that of the experimental results conducted in this project. The values of the lift curve slope of both results almost match. The drag coefficient values appear to be quite different. This may be due to unsatisfactory design and construction of the wing and the effect of the support struts, wing surface, and the connection between the wing and the struts. If the drag of the support arms and induced drag were calculated and removed from the total drag, this would get the measured drag(3D flow) in this project closer to that of the aerofoil from the NACA report(2D flow).

When the boundary layer trips were added to the wing, the results showed that lift coefficients of every BLT height located at 50%c from the leading edge are highest when compared to other positions. The results state that 6 mm height BLT located at 50%c produced lowest C_L while normal wing without BLT produced highest C_L for angles of attack between 0° and 14°. However, if the BLT height is lower than 6 mm, this makes the buffeting manner after stalling less severe because the laminar separation bubble transform to turbulent boundary layer and reattach to the wing surface making smaller the region of the LSB. This also results in the generation of more lift as the angle of attack is increased greater than 15°.

Drag coefficients of BLT height of 6, 4, 3, and 1.5 mm located at 50%c from the leading edge were compared to the wing without BLT. The results indicate that 4 mm height BLT generated the lowest C_D compared to all cases of both the normal wing and the wing with BLT.

For CFD simulations at Reynolds number of 650,000, the 2D NACA0015 aerofoil simulations with different turbulence models shows that the C_l slope is in good agreement with the 2D experimental results(NACA report No.586 [105]) from 0° to 9° of angle of attack. At an angle of attack greater than about 10° the result starts to have little difference from the NACA report. The obvious difference can be seen after 12°. Stall angle of the turbulence models are higher than that of the experiment. This is possibly due to the mesh

construction and the sharp trailing edge of the aerofoil in CFD simulation that is sharper than the aerofoil model tested in the NACA report No.586 [105].

The turbulence models also give higher drag coefficient than that from the experiment. The Cd is considerably different from the experimental results. This implies that the mesh construction was not built precisely for capturing the flow characteristics. The results show that these turbulence models cannot capture the flow well or as good as expected when the angle of attack is greater than 12°, where the strong adverse pressure gradient significantly affects the flow and causes it to separate from the aerofoil surface. It is recommended that DNS simulation should be applied to simulate the flow for better results.

6.2 Recommendations

As the surface of the wing was not smooth enough, this can be improved by more scrubbing the surface with sandpaper and then covering the wing surface with film or covering materials, for example, monokote to reduce skin friction drag of the wing. As a result, the total drag of the wing reduces and this makes it clearer to justify the effect of the boundary layer trips more precisely.

In this experiment, the air flow around the wing is three-dimensional flow because the wing is a finite wing. This forms induced drag due to wing tip vortices. Thus, it affects more the total drag in three-dimensional flow. If an aerofoil (infinite wing) or two-dimensional flow is required, this can be done either by extruding the ends of the aerofoil to the wind tunnel wall or attaching appropriate plates at the ends of the wing to reduce the tip-wing vortices effect, which generates induced drag. Furthermore, the connections around the aerofoil should be made as smooth as possible to reduce interference drag taking into account of the total drag.

For boundary layer trips, the tests were conducted for a few sizes of the trips and locations due to time constraint. It would have been better if smaller diameters of the trips as well as more locations of the trips were tested.

Flow visualization and pressure measurement are required to inspect the physical of the flow around the aerofoil/wing in more details. These allow more explanation what occur on the aerofoil/wing when attached with the boundary layer trips.

For CFD simulation, it would have been better if there were results from three-dimensional simulation both with and without the boundary layer trip on the aerofoil/wing to compare with. In addition, the mesh should be generated carefully to well capture the flow occurred. Either LES or DNS is required for better simulation in this case.

7. References

1. Lee, C. and Goldstein, D., Two-dimensional synthetic jet simulation, AIAA Journal, Vol. 40, No. 3, 2002, pp. 510–516.

2. Traub, L., Miller, A., and Rediniotis, O., Effects of Synthetic Jet Actuation on a Ramping NACA 0015 Airfoil, Journal of Aircraft, Vol. 41, No. 5, 2004, pp. 1153–1162.

3. Martin, P., Tung, C., Chandrasekhara, M., and Arad, E., Active Separation Control: Measurements and Computations for a NACA 0036 Airfoil,21 st AIAA Applied Aerodynamics Conference, 2003.

4. Renault, Renault Altica: 44MPG Diesel Concept with Active Airflow Management,2006,http://www.greencarcongress.com/2006/02/renault altica .html.

5. Chen, F. and Beeler, G., Virtual Shaping of a Two-Dimensional NACA 0015 Airfoil Using Synthetic Jet Actuator, AIAA Paper, Vol. 3273, No. 1, 2002.

6. Gad-el Hak, M., Modern developments in flow control, Appl. Mech. Rev, Vol. 49,No. 7, 1996, pp. 365–379.

7. Gad-el Hak, M., Flow Control: The Future, Journal of Aircraft, Vol. 38, No. 3, 2001,pp. 401.

8. Kitsios, V., Kotapati, R., Mittal, R., Ooi, A., Soria, J., and You, D., Numerical simulationof lift enhancement on a NACA 0015 airfoil using ZNMF jets, Proceedings of theSummer Program, 2006, pp. 457.

9. Schlichting, H. and Gersten, K., Boundary-Layer Theory, Springer, 2000.

10. Seifert, A., Darabi, A., and Wygnanski, I., Delay of Airfoil Stall by Periodic Excitation, Journal of Aircraft, Vol. 33, No. 4, 1996, pp. 691–698.

11. Duvigneau, R. and Visonneau, M., Simulation and Optimization of Aerodynamic Stall Control using a Synthetic Jet,2 nd AIAA Flow Control Conference, 2004.

12. Duvigneau, R. and Visonneau, M., Optimization of a synthetic jet actuator for aerodynamic stall control, Computers and Fluids, Vol. 35, No. 6, 2006, pp. 624–638.

13. Donovan, J., Krai, L., and Cary, A., Active Flow Control Applied to an Airfoil, AIAA Paper No, 1998, pp. 98–0210.

14. Patel, M., Kolacinski, R., Prince, T., Ng, T., and Cain, A., Flow Control Using Intelligent Control Modules for Virtual Aerodynamic Shaping, AIAA Paper, Vol. 3663, 2003.

15. Mallinson, S., Hong, G., and Reizes, J. A., Fundamental Studies of a Synthetic Jet Actuator, University of Technology Sydney, 13th Australian Fluid Mechanics Conference,1998.

16. Glezer, A. and Amitay,M., Synthetic Jets, Annual Review of Fluid Mechanics, Vol. 34,No. 1, 2002, pp. 503–529.

17. Vadillo, J., Numerical Study of Virtual Aerodynamic Shape Modification of an Airfoil Using a Synthetic Jet Actuator, Ph.D. thesis, Washington University, 2002.

18. El-Mistikawy, T., Separation prevention as an indirect problem based on the triple-deck theory, AIAA Journal, Vol. 32, No. 7, 1994, pp. 1423–1427.

19. Seifert, A., Theofilis, V., and Joslin, R., Issues in active flow control-Theory, simulation and experiment Proceedings, 2002.

20. Gilarranz, J., Traub, L., and Rediniotis, O., A New Class of Synthetic Jet Actuators-Part II: Application to Flow Separation Control, Journal of Fluids Engineering(Transactions of the ASME), Vol. 127, No. 2, 2005, pp. 377–387.

21. Bales, K., Khoo, P., and Jefferies, R., Flow Control of a NACA 0015 Airfoil Using a Chordwise Array of Synthetic Jets,41 st AIAA Aerospace Sciences Meeting &Exhibit, Reno, NV, 2003.

22. Huang, L., Huang, P., LeBeau, R., and Hauser, T., Numerical Study of Blowing and Suction Control Mechanism on NACA 0012 Airfoil, Journal of Aircraft, Vol. 41, No. 5,2004, pp. 1005–1013.

23. Utturkar, Y., Holman, R., Mittal, R., Carroll, B., Sheplak, M., and Cattafesta, L., A Jet Formation Criterion for Synthetic Jet Actuators, AIAA Paper, Vol. 636, 2003, pp. 2003.

24. Smith, B., The formation and evolution of synthetic jets, Physics of Fluids, Vol. 10, No. 9, 1998, pp. 2281.

25. Hamdani, H., Baig, A., and Zahir, S., A Systematic Study of Separation Control by Varying Various Parameters During Alternating Tangential Blowing/Suction, AIAA paper, Vol. 422, 2003.

26. Parekh, D., Glezer, A., Allen, M., Crittenden, T., and Birdsell, E., AVIA: Adaptive Virtual Aero surface, Defense Technical Information Center, 2004.

27. Wang, Z. and Stoffel, B., Behavior of synthetic jet on stalled airfoil flow, AIAA Paper, Vol. 222, 2003.

28. Kaya, M. and Tuncer, I. H., Response Surface Method for the Maximization of Thrust in Flapping Airfoils, AIAC-2007-011,4th Ankara International Aerospace Conference, 2007.

29. Anderson, John D., Jr., Fundamentals of Aerodynamics, Fourth Edition, Boston: McGraw-Hill, 2007.

30. Taylor HD., The elimination of diffuser separation by vortex generators, United Aircraft Corporation Report No. R-4012-3, June 1947.

31. Schubauer GB, Spangenber WG., Forced mixing in boundary layers, J of Fluid Mech, 1 1960; 8:10–32.

32. Bragg MB, Gregorek GM., Experimental study of airfoil performance with vortex generators, J of Aircraft 1987;24(5): 305–9.

33. Pearcey HH., Shock induced separation and its prevention by design and boundary-layer control, Boundary layer and flow control, vol. 2. New York: Pergamon Press, 1961. p. 1166–344.

34. Calarese W, et al., Afterbody drag reduction by vortex generators, AIAA Paper 85-0354, AIAA 23rd Aerospace Sciences Meeting, Reno, NV, January 14–17, 1985.

35. Brown AC, Nawrocki HF, Paley PN., Subsonic diffusers designed integrally with vortex generators, J Aircr 1968; 5(3):221–9.

36. Lin J C., Review of research on low-profile vortex generators to control boundary-layer separation, Progress in Aerospace Sciences 38, 2002; p 389- 420.

37. Kuethe AM., Effect of streamwise vortices on wake properties associated with sound generation, J Aircr 1972; 9(10):715–9.

38. Rao DM, Kariya TT., Boundary-layer submerged vortex generators for separation control—an exploratory study, AIAA Paper 88-3546-CP, AIAA/ASME/SIAM/APS 1st National Fluid Dynamics Congress, Cincinnati, OH, July 25–28, 1988.

39. Kerho M, et al., Vortex generators used to control laminar separation bubbles. Journal of Aircraft 1993;30(3):315–9.

40. Lin JC. et al., Separation control on high-lift airfoils via micro-vortex generators, J Aircr 1994;31(6):1317–23.

41. Klausmeyer S. et al., A flow physics study of vortex generator s on a multi- element airfoil, AIAA Paper 96-0548, 34th AIAA Aerospace Sciences Meeting and Exhibit, Reno, NV, January 15–18, 1996.

42. Ashill PR, Riddle GL., Control of leading-edge separation on a cambered delta wing, AGARD CP-548, March 1994. p 11-1–11-13.

43. Ashill PR, et al., Control of three dimensional separation on highly swept wings, ICAS-94- 4.6.2, September 1994.

44. Ashill PR, et al., Separation control on highly swept wings with fixed or variable camber, Aeronaut J. 1995;99(988):317–27.

45. Ashill PR, Fulker JL., A review of flow control research at DERA, Mechanics of Passive and Active Flow Control, IUTAM Symposium, Gottingen, Germany, September 7–11, 1998. p. 43–56.

46. Langan KJ, Samuels JJ., Experimental investigation of maneuver performance enhancements on an advanced fighter/attack aircraft, AIAA Paper 95-0442, AIAA 33rd Aerospace Sciences Meeting, Reno, NV, January 9–12, 1995.

47. McCormick DC., Shock–boundary layer interaction control with low-profile vortex generators and passive cavity, AIAA Paper 92-0064, 30th AIAA Aerospace Sciences Meeting and Exhibit, Reno, NV, January 6–9, 1992.

48. Holmes AE. et al., The application of sub-boundary layer vortex generators to reduce canopy Mach rumble interior noise on the Gulfstream III, AIAA Paper 87-0084, AIAA 25th Aerospace Sciences Meeting, Reno, NV, January 12–15, 1987.

49. Anabtawi AJ, et al., An experimental investigation of boundary layer ingestion in a diffusing S-duct with and without passive flow control, AIAA Paper 99-0739, 37th AIAA Aerospace Sciences Meeting and Exhibit, Reno, NV, January 11–14, 1999.

50. Anderson BH et al, A study on MEMS flow control for the management of engine face distortion in compact inlet systems, Third ASME/JSME

Joint Fluids Engineering Conference, ASME Paper FEDSM99-9620, July 1999.

51. Hamstra JW et al, Active inlet flow control technology demonstration, ICAS- 2000-6.11.2, 22nd International Congress of the Aeronautical Sciences, Harrogate, UK, August 27–September 1, 2000.

52. Tai TC., Effect of micro-vortex generators on V-22 aircraft forward-flight aerodynamics, AIAA Paper 2002-0553, 40th AIAA Aerospace Sciences Meeting and Exhibit, Reno, NV, January 14–17, 2002.

53. Lin J C. et al, Small submerged vortex generators for turbulent flow separation control, J of Spacecraft Rockets 1990;27(5):503–7.

54. Lin J C, et al., Investigation of several passive and active methods for turbulent flow separation control, AIAA Paper 90-1598, AIAA 21stFluid Dynamics, Plasma Dynamics and Lasers Conference, Seattle, WA, June 18–20, 1990.

55. Lin JC. et al., Exploratory study of vortex-generating devices for turbulent flow separation control, AIAA Paper 91-0042, AIAA 29th Aerospace Sciences Meeting, Reno, NV, January 7-10, 1991.

56. Lin JC., Control of turbulent boundary-layer separation using micro-vortex generators, AIAA Paper 99-3404, 30th AIAA Fluid Dynamics Conference, Norfolk, VA, June 28–July 1, 1999.

57. Jenkins L. et al., Flow control device evaluation for an internal flow with an adverse pressure gradient, AIAA Paper 2002-0266, 40th AIAA Aerospace Sciences Meeting and Exhibit, Reno, NV, January 14–17, 2002.

58. Ashill PR. et al., Research at DERA on sub boundary layer vortex generators (SBVGs), AIAA Paper 2001-0887, 39th AIAA Aerospace Sciences Meeting and Exhibit, Reno, NV, January 8–11, 2001.

59. Ashill PR. et al., Studies of flows induced by sub boundary layer vortex generators (SBVGs), AIAA Paper 2002-0968, 40th AIAA Aerospace Sciences Meeting and Exhibit, Reno, NV, January 14–17, 2002.

60. Wheeler GO., Low drag vortex generators, US Patent 5058837, 1991.

61. Yao C.S. et al., Flowfield measurement of device-induced embedded streamwise vortex on a flat plate, AIAA Paper 2002-3162, 1st AIAA Flow Control Conference, St. Louis, MO, June 24–27, 2002.

62. Allan BG. et al., Numerical simulation of vortex generator vanes and jets, AIAA Paper 2002-3160, 1st AIAA Flow Control Conference, St. Louis, MO, June 24–27, 2002.

63. Hao Li-Shu, et al., Airfoil flow control using vortex generators and a Gurney flap, Proceedings of the Institution of Mechanical Engineers, Part C: Journal of Mechanical Engineering Science, published online 5 March 2013.

64. G. Godard, M. Stanislas, Control of a decelerating boundary layer Part1: Optimization of passive vortex generators, Science direct, Aerospace Science and Technology 10 (2006) p. 181 – 191.

65. Nickerson J. D. Jr., A study of vortex generators at low Reynolds numbers, AIAA 24th Aerospace Sciences Meeting, January 6-9, 1986/Reno, Nevada.

66. Fernández-Gámiz U. et al., Computational study of the vortex path variation with the VG height, The Science of Making Torque from Wind 2014, Journal of Physics, Conference Series 524 (2014) 012024.

67. Angele K.P., Muhammad-Klingmann B., The effect of streamwise vortices on the turbulence structure of a separating boundary layer, European Journal of Mechanics B/Fluid 24 (2005) pp. 539-554.

68. U. Anand et al., Passive flow control over NACA0012 aerofoil using vortex generators, Proceedings of the 37th national & 4th international conference on Fluid Mechanics and fluid power, December 16-18, 2010, IIT Madras, Chennai, India.

69. Delnero J. S. et al, Vortex generator effect on low Reynolds number airfoils in turbulent flow, BBAA VI International Colloquium on: Bluff Bodies Aerodynamics& Applications, Milano, Italy, 20-24 July 2008.

70. H. Tebbiche and M. S. Boutoudj., Optimized vortex generators in the flow separation control around a NACA 0015 profile, Proceedings of the 9th International conference on structural dynamics, EURODYN 2014, Porto, Portugal, 30 June – 2 July 2014.

71. C M Velte et al, Flow analysis of vortex generators on wing sections by stereoscopic particle image velocimetry measurements, Environ. Res.Lett.3 (2008) 015006, 11pp.

72. Niels N. Sorensen, F. Zahle, C. Bak, T. Vronsky, Prediction of the effect of vortex generators on airfoil performance, The Science of Making

Torque from Wind 2014, Journal of Physics: Conference Series 524 (2014).

73. D. C. Montgomery, Design and analysis of experiments, John Wiley &Sons, New York, third edition, 1991.

74. F. T. Smith, Theoretical prediction and design for vortex generators in turbulent boundary layer, Journal of Fluid Mechanics 270 (1994) 91-131.

75. A. Tuck and J. Soria, Separation control on a NACA 0015 airfoil using a 2D micro ZNMF jet, Aircraft Engineering and Aerospace Technology: An International Journal 80/2 (2008), pp. 175-180.

76. Amitay, M. et al, Aerodynamic flow control over an conventional airfoil using synthetic jet actuators, AIAA Journal, Vol.39, No.3, March 2001.

77. Mc Cormick, D.C., Boundary layer separation control with directed synthetic jets, AIAA 2000-0519, 2000.

78. Gilarranz, J. L. and Rediniotis, O.K., Compact high-power synthetic jet actuators for flow separation control, AIAA 2001-0737, Proceeding 39th AIAA Aerospace Sciences Meeting and Exhibit, 2001.

79. Lyon, C. et al., Boundary layer trips on airfoils at low Reynolds numbers, AIAA 97-0511, 35th Aerospace Sciences Meeting &Exhibit, January 1997.

80. R. J. Howell and K. M. Roman, Loss reduction on ultra high lift low-pressure turbine blades using selective roughness and wake unsteadiness, Aeronautical Journal, vol.111, Issue 1118, 2007.

81. Vera, M. et al, The effects of a trip wire and unsteadiness on a high-speed highly loaded low-pressure turbine blade, Journal of Turbomachinery, October 2005, vol. 127, pp. 747-754.

82. Philippe Giguère and Michael S. Selig, Aerodynamic effects of leading edge tape on aerofoils at low Reynolds numbers, Wind Energy, Wind Energ.,2, 1999, pp.125-136.

83. Kwangmin Son et al, Mechanism of drag reduction by a surface trip wire on a sphere, J. of Fluid Mechanics (2011), vol.672, pp. 411-427.

84. Chi Wai Wong et al, Bubble burst control for stall suppression on a NACA 63_1-012 airfoil, AIAA 2009-1111, 47th AIAA Aerospace Sciences Meeting, 5-8 January, 2009.

85. A. F. Huber II and T. J. Mueller, The effect of trip wire roughness on the performance of the Wortmann FX 63-137 airfoil at low Reynolds numbers, Experiment in Fluid Mechanics 5, 1987, pp. 263-272.

86. L. P. Erm et al, Boundary layer trip size selection on streamlined bodies of revolution, 18th Australasian Fluid Mechanics Conference, Australia, December 2012.

87. Fushui Guo, Experimental study of the behaviour of the synthetic jets for effective flow separation control, PhD Thesis, 2010.

88. Lissaman, P. B. S., Low Reynolds number airfoils, Annual Review Fluid Mechanics, vol.15, 1983, pp. 223-239.

89. Schlichting, H. and Gesten, K., Boundary layer theory, Ed.8, Springer, 2000.

90. King, P. A. and Breuer, K. S., Oblique transition in a laminar Blasius boundary layer, Journal of Fluid Mechanics, Vol.453, 2002, pp.177-200.

91. Mueller, T. J. and Brendel, M., Boundary layer measurements on an airfoil at a low Reynolds number in an oscillating freestream, AIAA Journal 26, 3, 1988, pp. 257- 263.

92. Lee et al, Numerical study on aerodynamic characteristic of NACA0015, Applied Mechanics and Materials, Vol. 302, 2013, pp. 640-645.

93. http://www.cfd-online.com/Tools/yplus.php.

94. Abbott, I.H. and von Doenhoff, A.E., Theory of Wing Sections, Dover Publications Inc., New York, 1959.

95. Delery, J.M., Shock wave/turbulent boundary layer interaction and its control, Progress in Aerospace Sciences, Vol. 22, No. 4, 1985, pp. 209-280.

96. Kral, L.D., Active flow control technology, ASME Fluids Engineering Technical Brief, 2000.

97. Lachmann, G.V., Boundary Layer and Flow Control: Its Principles and Application.Vol. 1, Pergrmon Press, 1961.

98. Johari, H. and McManus, K.R., Visualization of pulsed vortex generator jets for active control of boundary layer separation, AIAA 1997-2021, 28th Fluid Dynamics Conference, Snowmass Village, USA, 29 June - 2 July 1997.

99. Moin, P. and Bewley, T., Feedback control of turbulence, Applied Mechanics Reviews. Vol. 47, No. 6, 1994, pp. S3-S13.

100. Prandtl, L., Über Flüssigkeitbewegung bei sehr kleiner Reibung (On the motion of fluid with very small viscosity), Proceedings of the 3rd International Mathematical Congress, Heidelberg, Germany, 1904, pp. 484-491.

101. Viswanath, P.R., Shockwave-turbulent boundary layer interaction and its control: A survey of recent developments, Sadhana, Vol. 12, No. 1-2, 1988, pp. 45-104.

102. Wallis, R.A., The use of air jets for boundary layer control, Aerodynamics Research Laboratories, Australia, Aero Note 110, 1952.

103. Warsop, C., MEMS and Microsystems technologies – their potential and status for drag reduction and separation control, European Congress on Computational Methods in Applied Science and Engineering (ECCOMAS), Jyväskylä, Finland, 24-28 July 2004.

104. Wood, N.J., Sadri, A.M. and Crook, A., Control of turbulent flow separation by synthetic jets, AIAA 2000-4331, 18th AIAA Applied Aerodynamics Conference, Denver, USA, 14-17 August 2000.

105. Eastman N. Jacobb and Albert Sherman, Airfoil section characteristics as affected by variations of the Reynolds number, NACA report No.586.